

Quasiparticle spin relaxation with superconducting velocity-tunable state in GaAs(100) quantum wells in proximity to *s*-wave superconductor

T. Yu and M. W. Wu*

*Hefei National Laboratory for Physical Sciences at Microscale, Department of Physics,
and CAS Key Laboratory of Strongly-Coupled Quantum Matter Physics, University of Science and Technology of China,
Hefei, Anhui, 230026, China*

(Received 28 July 2016; revised manuscript received 6 October 2016; published 16 November 2016)

We investigate the quasiparticle spin relaxation with superconducting-velocity-tunable state in GaAs (100) quantum wells in proximity to an *s*-wave superconductor. We first present the influence of the supercurrent on the quasiparticle state in GaAs (100) quantum wells, which can be tuned by the superconducting velocity. Rich features such as the suppressed Cooper pairings, large quasiparticle density and nonmonotonically tunable momentum current can be realized by varying the superconducting velocity. In the degenerate regime, the quasiparticle Fermi surface is composed by two arcs, referred to as Fermi arcs, which are contributed by the electron- and holelike branches. The D'yakonov-Perel' spin relaxation is then explored, and intriguing physics is revealed when the Fermi arc emerges. Specifically, when the order parameter tends to zero, it is found that the branch-mixing scattering is forbidden in the quasidelectron band. When the condensation process associated with the annihilation of the quasidelectron and quasihole is *slow*, this indicates that the electron- and holelike Fermi arcs in the quasidelectron band are independent. The open structure of the Fermi arc leads to the nonzero angular average of the effective magnetic field due to the spin-orbit coupling, which acts as an effective Zeeman field. This Zeeman field leads to spin oscillations even in the strong-scattering regime. Moreover, in the strong-scattering regime, we show that the open structure of the Fermi arc also leads to the insensitiveness of the spin relaxation to the momentum scattering, in contrast to the conventional motional narrowing situation. Nevertheless, with a *finite* order parameter, the branch-mixing scattering can be triggered, opening the interbranch spin relaxation channel, which is dominant in the strong-scattering regime. In contrast to the situation with an extremely small order parameter, due to the interbranch channel, the spin oscillations vanish and the spin relaxation exhibits a motional narrowing feature in the strong-scattering regime.

DOI: [10.1103/PhysRevB.94.205305](https://doi.org/10.1103/PhysRevB.94.205305)

I. INTRODUCTION

In recent years, the superconducting spintronics has attracted much attention for providing new methods to control over the spin degree of freedom based on the spin-triplet Cooper pairs and Bogoliubov quasiparticles [1–3]. On one hand, the triplet Cooper pairs combine both the features of the spintronics [4–11] and superconductivity, offering the possibility to realize the spin-polarized supercurrent [1–3,12–17]. On the other hand, as the quasiparticle charge depends on its momentum in a conventional superconductor, which is exactly zero at the Fermi momentum, it is promising to tune the spin degree of freedom with a weak disturbance on the charge one in one system [18–32]. To reveal the physics in the superconducting spintronics, the spin dynamics for both the spin-polarized Cooper pairs and quasiparticles has been intensively studied [1–3,18–34].

Specifically, for the quasiparticle, rich physics has been reported in the studies on the charge or spin injection from a nonmagnetic metal or ferromagnet to a conventional superconductor [18–20,22–29,31,32]. It is shown that the injection of one electron with charge e into the superconductor can add one Cooper pair with charge $2e\tilde{v}_k^2$ and spin 0 and a quasiparticle with charge $e(\tilde{u}_k^2 - \tilde{v}_k^2)$ and spin $1/2$, respectively [19,20,25,26,28,32]. Here, $\tilde{u}_k^2 = 1/2 + \tilde{\zeta}_k/(2E_k)$

and $\tilde{v}_k^2 = 1/2 - \tilde{\zeta}_k/(2E_k)$, in which $\tilde{\zeta}_k = \epsilon_k - \mu_S$ with ϵ_k represent the kinetic energy of the electron and μ_S is the chemical potential in the superconductor; $E_k = \sqrt{\tilde{\zeta}_k^2 + |\Delta_S|^2}$ denotes the energy spectrum of the quasiparticle with Δ_S being the superconducting order parameter. Accordingly, in the steady state, the injected charge and spin are mainly carried by the Cooper pairs and quasiparticles separately, indicating that the spin-charge separation can be realized during the injection [2,27–29,35]. It is further noticed that in the process of the charge and spin injections, nonequilibrium charge and/or spin imbalance can be created [18,19,28,29,36,37]. It is then revealed that in the dynamical process, to maintain the charge neutrality, the Cooper pair condensate can respond to the dynamics of the injected quasiparticles [18,20,24,25,28,32]. Accordingly, the study on the quasiparticle dynamics itself is essential to further reveal the dynamics of Cooper pairs.

Among the quasiparticle dynamics, the spin dynamics in the superconducting metals has been studied both theoretically [18,21] and experimentally [26,27,32]. Theoretically, the quasiparticle spin relaxation has been calculated by considering the spin-flip [18,21] and spin-orbit scatterings due to the impurities [18], which lies in the Elliott-Yafet mechanism [38,39]. In the superconducting state, it is shown that the spin-flip scattering is efficiently enhanced due to the enhancement of the density of states (DOS) [18,21]. Whereas the spin-orbit scattering is efficiently suppressed due to the coherence factor $\tilde{\zeta}_k/E_k$ in the scattering term [18]. Experimentally, long injection lengths were reported for spin injected

*Corresponding author: mwwu@ustc.edu.cn

into superconducting Al [26,27] and Nb [31], indicating a long spin relaxation time (SRT) in the superconducting state compared to the normal one. Furthermore, it is further found that the injected spin current in the superconducting Al can significantly influence the quasiparticle SRT, with the spin relaxation behavior in the superconducting state resembling the normal one when the injected spin current is large [31]. As rich physics is revealed in the Elliott-Yafet mechanism in the superconducting metal, it is intriguing to study the D'yakonov-Perel' (DP) mechanism [40], which is more important for materials without center-inversion symmetry, in the superconducting state. Furthermore, proximity-induced superconductivity has been realized in InAs [41–43] and GaAs [44–46] heterostructures, offering the chance to study the DP mechanism in the superconducting semiconductors.

It is noted that in the study of the dynamics in a superconducting system, different kinetic equations based on the quasiclassical [13–15,47–62] and quasiparticle [18,21,63–72] approximations are used. The quasiclassical approximation is applicable for a system with a large Fermi energy, in which the dependence on the momentum magnitude is neglected in the Green function, whereas the frequency and angle-of-momentum dependencies are explicitly considered. For the quasiparticle approximation, in the Green function, the dependencies on the angle and magnitude of the momentum are explicitly considered, but the frequency dependence is not emphasized. Moreover, this approximation is applicable only when the perturbation on the superconducting order parameter is not strong, and hence the quasiparticle energy spectrum is well defined [57,64,67]. To the best of our knowledge, the quasiparticle approximation is mainly applied to systems without the SOC [18,21,63–70]. When the SOC exists, Einzel *et al.* derived a kinetic equation based on the quasiparticle approximation, nevertheless, in which the scattering is not considered [71,72]. Kinetic equations of quasiparticles with the scattering term explicitly considered in the presence of the SOC are still absent, even for the simplest case with the *s*-wave order parameter.

In this work, we investigate the DP spin relaxation with a superconducting-velocity-tunable quasiparticle state in GaAs (100) quantum wells (QWs) in proximity to an *s*-wave superconductor. The influence of the supercurrent on the quasiparticle state is first addressed in the superconducting QWs, based on which the quasiparticle spin relaxation is then explored. In the *s*-wave superconductor, the order parameter, i.e., $\Delta_S = |\Delta_S|e^{i\Lambda}$, is contributed by its magnitude $|\Delta_S|$ and superconducting phase Λ . Then, due to the superconducting proximity effect [16,73–76], by assuming that the superconducting phase is not disrupted by the disorder, an *s*-wave order parameter with the same superconducting phase at the superconductor-semiconductor interface but different magnitude $|\Delta|$ can arise in the semiconductor. Specifically, with the inhomogeneous superconducting phase, a superconducting velocity $\mathbf{v}_s = \nabla\Lambda/m^* \equiv \mathbf{q}/m^*$ arises with m^* being the electron effective mass in the QWs [77,78]. Here, it is assumed that \mathbf{v}_s is perpendicular to the growth direction of QWs, from which a supercurrent is induced. In this work, it is further assumed that the superconducting velocity is small, which marginally influences the superconducting state in the *s*-wave superconductor [77,78]. However, when $|\Delta| \ll |\Delta_S|$,

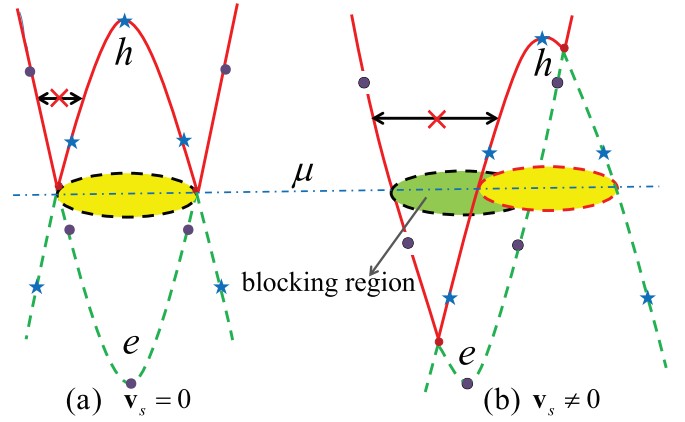


FIG. 1. Schematic showing the tilt of the quasiparticle energy spectrum and the formation of the blocking region. Here, $|\Delta|$ is taken to be extremely small. In (a) [(b)], $\mathbf{v}_s \equiv \mathbf{q}/m^* = 0$ ($\mathbf{v}_s \neq 0$). The red solid (green dashed) curves represent the quasielectron (quasihole) energy spectrum; whereas the curve labeled by the dots (stars) denotes the electron (hole) band. In (b), compared to (a), due to the superconducting velocity, the electron and hole bands are shifted by $\mathbf{q}/2$ and $-\mathbf{q}/2$, respectively, and hence the resulting quasielectron energy spectrum is tilted. When the quasielectron energy is tilted to be smaller than the chemical potential μ represented by the blue chain line, the blocking region emerges, which is represented by the green crescent shape in (b). Finally, it is addressed that with $|\Delta|$ tending to zero, the branch-mixing scattering due to the impurity (represented by the black arrow) is forbidden without and with the supercurrent.

the superconducting velocity can efficiently tune the superconducting state in QWs. It is noted that the influence of the supercurrent on the proximity effect between the superconductor and semiconductor was first theoretically predicted [79,80] and then experimentally confirmed [43]: in the semiconductor in proximity to the *s*-wave superconductor, the diamagnetic supercurrent induced by the magnetic field can cause the Doppler shift for the quasiparticle state in the semiconductor.

We show that in the superconducting QWs, the superconducting velocity can cause the tilt of the quasiparticle energy spectrum. Specifically, in the presence of the supercurrent, the energy spectra of the quasielectron (+) and quasihole (−) are

$$E_{\mathbf{k}}^{\pm} = \mathbf{k} \cdot \mathbf{v}_s/2 \pm \mathcal{E}_{\mathbf{k}}. \quad (1)$$

Here, $\mathcal{E}_{\mathbf{k}} = \sqrt{\epsilon_{\mathbf{k}}^2 + |\Delta|^2}$ with $\epsilon_{\mathbf{k}} = k^2/(2m^*) + m^*v_s^2/8 - \mu$ with μ being the chemical potential in the semiconductor ($\hbar \equiv 1$ throughout this paper). It is noted that the chemical potential is shifted by $-m^*v_s^2/8$ due to the superconducting velocity. From Eq. (1), for the quasielectron band, when $|\Delta| \rightarrow 0$, $E_{\mathbf{k}}^+ \approx (\mathbf{k} + \mathbf{q}/2)^2/(2m^*) - \mu$ if $|\mathbf{k}| > k_F$ and $E_{\mathbf{k}}^+ \approx -(\mathbf{k} - \mathbf{q}/2)^2/(2m^*) + \mu$ if $|\mathbf{k}| < k_F$. With the former and latter branches referred to as the electron- ($\zeta_{\mathbf{k}} > 0$ with negative charge) and holelike ($\zeta_{\mathbf{k}} < 0$ with positive charge) branches, it can be seen that the superconducting velocity leads to shifts of the electron- and holelike branches by $\mathbf{q}/2$ and $-\mathbf{q}/2$ (i.e., the Doppler shift [43,79,80]), respectively. Then the tilt of the quasiparticle energy spectrum can be simply understood.

In Fig. 1(a) [Fig. 1(b)], the quasielectron (quasihole) energy spectrum is schematically plotted with $|\Delta| \rightarrow 0$ when

$\mathbf{v}_s \equiv \mathbf{q}/m^* = 0$ ($\mathbf{v}_s \neq 0$) by the red solid (green dashed) curves. It can be seen that the quasielectron (quasihole) band is composed by the positive (negative) parts of the electron and hole bands, shown by the curves labeled by the dots and stars. Due to the superconducting velocity, compared to Fig. 1(a), the electron and hole-bands are shifted by $\mathbf{q}/2$ and $-\mathbf{q}/2$, respectively, and hence the resulting quasiparticle energy spectrum is tilted [Fig. 1(b)]. Specifically, the tilted excitation energy can be even smaller than the chemical potential μ , represented by the blue chain line in Fig. 1. Accordingly, the quasielectrons mainly populate the region with the negative excitation energy even at zero temperature, which is referred to as the blocking region [81,83]. In Fig. 1(b), the blocking region for the quasielectron is schematically represented by the green “crescent,” whose formation can be treated as the shift of the Fermi surfaces of the electron and hole. The appearance of the blocking region can significantly influence the Cooper pairings, the quasiparticle density, and the momentum current driven by the supercurrent in QWs [77,78,81–83].

Specifically, we show that driven by the supercurrent, the center-of-mass momentum \mathbf{q} is carried by the Cooper pairs, with the anomalous correlations only existing between the states with momentum $\mathbf{k} + \mathbf{q}/2$ and $-\mathbf{k} + \mathbf{q}/2$. Moreover, we show that the anomalous correlations around the Fermi surface are efficiently suppressed due to the emergence of the blocking region (refer to Sec. III B 1). Furthermore, the quasiparticle density increases with the increase of the superconducting velocity. In this process, the system experiences a crossover between the nondegenerate and degenerate limits. Finally, it is revealed that when the blocking region appears, the momentum current contributed by the quasiparticles flows in the opposite direction to the one due to the Cooper pairs. Accordingly, due to the competition of the Cooper pairs and quasiparticles in the blocking region, there exists a peak in the superconducting-velocity dependence of the momentum current, whose position corresponds to the appearance of the blocking region.

We then study the quasiparticle spin relaxation in the superconducting QWs. Based on the quasiparticle approximation due to the small Fermi energy in QWs, the kinetic spin Bloch equations (KSBEs) [4,9] for the quasiparticle are set up with the SOC and quasiparticle-impurity scattering explicitly considered. By using the KSBEs, we calculate the SRT without and with the superconducting velocity, respectively. Rich physics is revealed. Without the supercurrent, we address that the branch-mixing scattering [36,37] due to the impurity represented by the black arrow in Fig. 1(a) is forbidden. Here, the branch-mixing scattering is referred to as the scattering of quasiparticles between the electronlike and holelike branches [36,37]. This indicates that the electron- and holelike branches are independent and hence only the intrabranched spin relaxation channel exists. In this situation, when $|\Delta|$ tends to zero, the SRT recovers to the normal one. Whereas with a finite order parameter, it is found that in the superconducting state, no matter whether the scattering is weak or strong, the SRT is enhanced compared to the normal one, whereas the boundary between the weak- and strong-scattering regimes is unchanged. This comes from the efficient suppressions of the SOC and impurity scattering for the quasiparticle by the same factor $|\epsilon_{\mathbf{k}}|/\mathcal{E}_{\mathbf{k}}$.

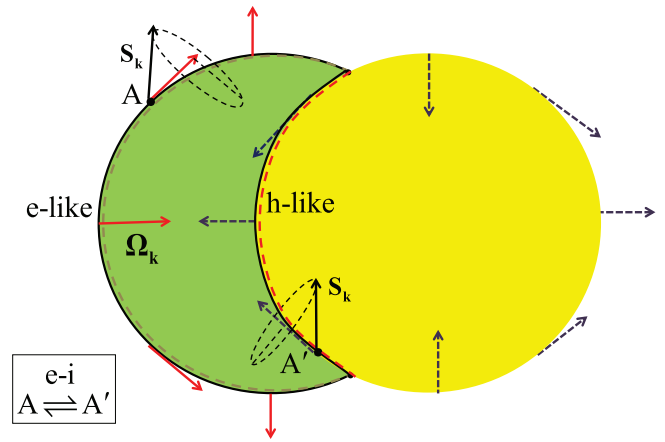


FIG. 2. Schematic of the intra- and interbranch spin relaxation processes. The blocking region is represented by the green area in the crescent shape. Around the blocking region, its left (right) boundary represented by the gray (red) dashed curve mainly comes from the electron(hole) band, which is referred to as the electron(hole)like Fermi arc in this work. Around the electron- and holelike Fermi arcs, the red solid and blue dashed arrows denote the effective magnetic field due to the SOC (i.e., $\Omega_{\mathbf{k}}$). With an extremely small order parameter, the branch-mixing scattering is forbidden, and the spin polarization in the electron- and holelike bands relaxes independently. This is referred to as the intrabranched spin relaxation. Whereas with the finite order parameter, when the blocking region emerges, the quasiparticles can be efficiently scattered between the left and right boundaries of the blocking region (e.g., scattering from A to A'), triggering the branch-mixing scattering [36,37]. This opens the interbranch spin relaxation channel.

With the supercurrent, the quasiparticle spin relaxations with extremely small ($|\Delta| \ll 0.1$ meV) and finite ($|\Delta| \gtrsim 0.1$ meV) order parameters are explored. When the order parameter is extremely small (e.g., $|\Delta| = 0.01$ meV), the branch-mixing scattering is still forbidden [refer to Fig. 1(b)]. This is because the coherence factor ($\approx \epsilon_{\mathbf{k}}/|\epsilon_{\mathbf{k}}| + \epsilon_{\mathbf{k}'}/|\epsilon_{\mathbf{k}'}|$) in the quasiparticle-impurity scattering tends to zero. However, differing from the situation without the supercurrent, when the blocking region emerges, the Fermi surfaces from the electron- and holelike branches are *not closed*, referred to as “Fermi arcs.” In Fig. 2, the Fermi arcs from the electron- and holelike branches are represented by the gray and red dashed curves in the left and right boundaries of the blocking region. One observes that in the electron- or holelike Fermi arc, the angular average of the effective magnetic field due to the SOC (i.e., $\Omega_{\mathbf{k}}$) is not zero. When the condensation process is slow, which can be associated with the annihilation of quasielectron and quasihole [84–86], the spin polarization mainly relaxes within the Fermi arcs.

It is revealed that the quasiparticle spin relaxation at the Fermi arc exhibits anomalous features in the *strong* scattering regime. Specifically, on one hand, the spin oscillations can be induced by the superconducting velocity; on the other hand, the spin relaxation becomes *insensitive* to the momentum scattering. The latter phenomenon is in contrast to the conventional DP relaxation, where the spin relaxation is suppressed by the momentum scattering (motional narrowing effect [40]). We reveal that the nonzero angular average of the SOC in one Fermi

arc corresponds to an effective Zeeman field. This effective Zeeman field can cause the spin oscillations even in the strong scattering regime, which nevertheless has little influence on the spin relaxation. Actually, this feature provides a direct proof for the existence of the Fermi arc. It is further shown that by switching off the effective Zeeman field, the magnitude of the residue effective magnetic field *strongly* depends on the direction of the momentum, causing an effective modular-dependent inhomogeneous broadening [9,87] even for the elastic scattering. This modular-dependent inhomogeneous broadening can be enhanced by the momentum scattering in the strong-scattering regime and tends to enhance the spin relaxation. Nevertheless, the motional narrowing effect tends to suppress the spin relaxation [40]. Thus the competition of the two opposite trends leads to the insensitiveness of momentum scattering dependence of the SRT in the strong-scattering regime.

When the order parameter is big enough (i.e., $|\Delta| \gtrsim 0.1$ meV in our model), in the presence of the supercurrent, it is revealed that the tilt of the energy spectrum can trigger the branch-mixing scattering. In this situation, there exist the intra- and interbranch spin relaxation channels for the quasiparticle spin relaxation, as illustrated in Fig. 2. Furthermore, we reveal the role of the intra- and interbranch spin relaxation channels on the spin relaxation in both the weak- and strong scattering regimes. Specifically, in the weak-scattering regime, the intrabranch spin relaxation channel is dominant; whereas in the strong-scattering regime, the interbranch channel becomes dominant when the blocking region appears. Moreover, in the strong-scattering regime, with the branch-mixing scattering efficiently triggered, the quasielectron can feel all the SOC around the Fermi surface, whose angular average is zero (refer to Fig. 2). Accordingly, in the strong-scattering regime, in contrast to the situation with extremely small order parameter, no spin oscillation occurs. Furthermore, in this situation, the inhomogeneous broadening becomes the conventional one and hence the spin relaxation is suppressed by the momentum scattering, exhibiting the motional narrowing feature.

This paper is organized as follows. We first lay out the Hamiltonian in Sec. II. In Sec. III, we analyze the quasiparticle state in the superconducting QWs both analytically (Sec. III A) and numerically (Sec. III B). In Sec. IV, the quasiparticle spin relaxation is studied by using the KSBEs, derived in the quasiparticle approximation. We conclude and discuss in Sec. V.

II. HAMILTONIAN

In this section, we present the Hamiltonian of the symmetric (100) QWs in proximity to an s -wave superconductor. In the particle space, the Hamiltonian is composed by the Bogoliubov-de Gennes (BdG) Hamiltonian and electron-impurity interaction. The BdG Hamiltonian is written as [16,73–76]

$$H_0 = \int \frac{d\mathbf{r}}{2} \Phi^\dagger(\mathbf{r}) \begin{pmatrix} \zeta_{\mathbf{k}} & h_{\mathbf{k}} & 0 & \Delta(\mathbf{r}) \\ h_{\mathbf{k}}^* & \zeta_{\mathbf{k}} & -\Delta(\mathbf{r}) & 0 \\ 0 & -\Delta^*(\mathbf{r}) & -\zeta_{\mathbf{k}} & h_{\mathbf{k}}^* \\ \Delta^*(\mathbf{r}) & 0 & h_{\mathbf{k}} & -\zeta_{\mathbf{k}} \end{pmatrix} \Phi(\mathbf{r}), \quad (2)$$

where $\Phi(\mathbf{r})$ is the particle field operator. Here, $\zeta_{\mathbf{k}} = k^2/(2m^*) - \mu$; $h_{\mathbf{k}} = -\alpha k_x - i\alpha k_y$ comes from the Dresselhaus SOC, [88] in which $\alpha = \gamma_D(\pi/a)^2$ for the infinitely deep well with γ_D and a being the Dresselhaus coefficient and well width, respectively; $\Delta(\mathbf{r}) = |\Delta|e^{i\mathbf{q}\cdot\mathbf{r}}$ is the s -wave order parameter. Specifically, $|\Delta|$ and \mathbf{q} are assumed to be homogeneous in this work.

The electron-impurity interaction is expressed as

$$H_{\text{im}} = \frac{1}{2} \int d\mathbf{r} \Phi^\dagger(\mathbf{r}) V(\mathbf{r}) \tau_3 \Phi(\mathbf{r}), \quad (3)$$

with $\tau_3 \equiv \text{diag}(1, 1, -1, -1)$ and $V(\mathbf{r})$ denoting the screened Coulomb potential, whose Fourier component $V_{\mathbf{k}} = V_{\mathbf{k}}^0/(1 - P_{\mathbf{k}}^{(1)} V_{\mathbf{k}}^0)$. Here, $V_{\mathbf{k}}^0 = \int dy \frac{1}{\pi a} |I(y)|^2 \frac{e^2}{\varepsilon_0 \kappa_0 (k^2 + 4y^2/a^2)}$, with ε_0 and κ_0 representing the vacuum permittivity and relative dielectric constant; $|I(y)|^2 = \frac{\pi^4 \sin^2(y)}{(\pi^2 - y^2)^2 y^2}$ standing for the form factor; $P_{\mathbf{k}}^{(1)}$ denoting the longitudinal polarization function, whose expression has been derived in Ref. [16].

In the momentum space, the BdG Hamiltonian is further represented as

$$H_0(\mathbf{k}) = \frac{1}{2} \sum_{\mathbf{k}} \Phi_{\mathbf{k}}^\dagger \begin{pmatrix} \zeta_{\mathbf{k}+\frac{\mathbf{q}}{2}} & h_{\mathbf{k}+\frac{\mathbf{q}}{2}} & 0 & |\Delta| \\ h_{\mathbf{k}+\frac{\mathbf{q}}{2}}^* & \zeta_{\mathbf{k}+\frac{\mathbf{q}}{2}} & -|\Delta| & 0 \\ 0 & -|\Delta| & -\zeta_{\mathbf{k}-\frac{\mathbf{q}}{2}} & h_{\mathbf{k}-\frac{\mathbf{q}}{2}}^* \\ |\Delta| & 0 & h_{\mathbf{k}-\frac{\mathbf{q}}{2}} & -\zeta_{\mathbf{k}-\frac{\mathbf{q}}{2}} \end{pmatrix} \Phi_{\mathbf{k}},$$

where $\Phi_{\mathbf{k}}^\dagger = (a_{\mathbf{k}+\frac{\mathbf{q}}{2}\uparrow}^\dagger, a_{\mathbf{k}+\frac{\mathbf{q}}{2}\downarrow}^\dagger, a_{-\mathbf{k}+\frac{\mathbf{q}}{2}\uparrow}, a_{-\mathbf{k}+\frac{\mathbf{q}}{2}\downarrow})$; the electron-impurity interaction is written as

$$H_{\text{im}} = \frac{1}{2} \sum_{\mathbf{k}\mathbf{k}'} \Phi_{\mathbf{k}}^\dagger V_{\mathbf{k}-\mathbf{k}'} \tau_3 \Phi_{\mathbf{k}'}. \quad (4)$$

We then transform the Hamiltonian in particle space to the quasiparticle one by using the transformation

$$U_{\mathbf{k}} = \begin{pmatrix} u_{\mathbf{k}} & 0 & 0 & v_{\mathbf{k}} \\ 0 & u_{\mathbf{k}} & -v_{\mathbf{k}} & 0 \\ 0 & v_{\mathbf{k}} & u_{\mathbf{k}} & 0 \\ -v_{\mathbf{k}} & 0 & 0 & u_{\mathbf{k}} \end{pmatrix}. \quad (5)$$

Here, $u_{\mathbf{k}} = \sqrt{\frac{1}{2} + \frac{\epsilon_{\mathbf{k}}}{2\mathcal{E}_{\mathbf{k}}}}$ and $v_{\mathbf{k}} = \sqrt{\frac{1}{2} - \frac{\epsilon_{\mathbf{k}}}{2\mathcal{E}_{\mathbf{k}}}}$. Then in the quasiparticle space, the field operator is denoted as $\Psi_{\mathbf{k}} \equiv (\alpha_{\mathbf{k}\uparrow}, \alpha_{\mathbf{k}\downarrow}, \alpha_{-\mathbf{k}\uparrow}^\dagger, \alpha_{-\mathbf{k}\downarrow}^\dagger)^T = U_{\mathbf{k}} \Phi_{\mathbf{k}}$. Accordingly, the BdG Hamiltonian in the quasiparticle space is written as

$$H_0^q(\mathbf{k}) = \begin{pmatrix} \mathbf{k} \cdot \frac{\mathbf{v}_s}{2} + \mathcal{E}_{\mathbf{k}} & \frac{\epsilon_{\mathbf{k}}}{\mathcal{E}_{\mathbf{k}}} h_{\mathbf{k}} + h_{\frac{\mathbf{q}}{2}} & -\frac{|\Delta|}{\mathcal{E}_{\mathbf{k}}} h_{\mathbf{k}} & 0 \\ \frac{\epsilon_{\mathbf{k}}}{\mathcal{E}_{\mathbf{k}}} h_{\mathbf{k}}^* + h_{\frac{\mathbf{q}}{2}}^* & \mathbf{k} \cdot \frac{\mathbf{v}_s}{2} + \mathcal{E}_{\mathbf{k}} & 0 & \frac{|\Delta|}{\mathcal{E}_{\mathbf{k}}} h_{\mathbf{k}}^* \\ -\frac{|\Delta|}{\mathcal{E}_{\mathbf{k}}} h_{\mathbf{k}}^* & 0 & \mathbf{k} \cdot \frac{\mathbf{v}_s}{2} - \mathcal{E}_{\mathbf{k}} & \frac{\epsilon_{\mathbf{k}}}{\mathcal{E}_{\mathbf{k}}} h_{\mathbf{k}}^* - h_{\frac{\mathbf{q}}{2}}^* \\ 0 & \frac{|\Delta|}{\mathcal{E}_{\mathbf{k}}} h_{\mathbf{k}} & \frac{\epsilon_{\mathbf{k}}}{\mathcal{E}_{\mathbf{k}}} h_{\mathbf{k}} - h_{\frac{\mathbf{q}}{2}} & \mathbf{k} \cdot \frac{\mathbf{v}_s}{2} - \mathcal{E}_{\mathbf{k}} \end{pmatrix}. \quad (6)$$

The electron-impurity interaction Hamiltonian is transformed to be

$$H_{\text{im}} = \frac{1}{2} \sum_{\mathbf{k}\mathbf{k}'} \Psi_{\mathbf{k}}^\dagger V_{\mathbf{k}'-\mathbf{k}}^q \Psi_{\mathbf{k}'}, \quad (7)$$

where the impurity potential

$$V_{\mathbf{k}'-\mathbf{k}}^q = V_{\mathbf{k}-\mathbf{k}'} \begin{pmatrix} A_{\mathbf{k}\mathbf{k}'} & 0 & 0 & B_{\mathbf{k}\mathbf{k}'} \\ 0 & A_{\mathbf{k}\mathbf{k}'} & -B_{\mathbf{k}\mathbf{k}'} & 0 \\ 0 & -B_{\mathbf{k}\mathbf{k}'} & -A_{\mathbf{k}\mathbf{k}'} & 0 \\ B_{\mathbf{k}\mathbf{k}'} & 0 & 0 & -A_{\mathbf{k}\mathbf{k}'} \end{pmatrix}, \quad (8)$$

with $A_{\mathbf{k}\mathbf{k}'} = u_{\mathbf{k}}u_{\mathbf{k}'} - v_{\mathbf{k}}v_{\mathbf{k}'}$ and $B_{\mathbf{k}\mathbf{k}'} = u_{\mathbf{k}}v_{\mathbf{k}'} + v_{\mathbf{k}}u_{\mathbf{k}'}$.

III. SUPERCONDUCTING-VELOCITY-TUNABLE QUASIPARTICLE STATE IN QWs

In this section, we analyze the quasiparticle state in the superconducting QWs, which can be tuned by the superconducting velocity, first analytically (Sec. III A) and then numerically (Sec. III B).

A. Analytical analysis

In this part, we analytically analyze the quasiparticle state by using the equilibrium Green function at the Matsubara representation [89–91]. In the derivation, the SOC is neglected as it is much weaker compared to the kinetic energy.

In the particle space, the equilibrium Green function at the Matsubara representation is defined as $\tilde{G}_{12} = -i\langle T_{\tau} \tilde{\Phi}_1 \tilde{\Phi}_2^{\dagger} \rangle$ [89–91], in which T_{τ} represents the chronological product, $(1) = (\tau_1, \mathbf{r}_1)$ is the imaginary time-space point, $\langle \dots \rangle$ denotes the ensemble average, and $\tilde{\Phi}(t, \mathbf{r}) \equiv e^{i\tau_3 \Delta(t, \mathbf{r})/2} \Phi(t, \mathbf{r})$. The Green function in the frequency-momentum space is derived to be

$$\tilde{G}(i\omega_n, \mathbf{k}) = \begin{pmatrix} A(i\omega_n, \mathbf{k}) & 0 & 0 & C(i\omega_n, \mathbf{k}) \\ 0 & A(i\omega_n, \mathbf{k}) & -C(i\omega_n, \mathbf{k}) & 0 \\ 0 & -C(i\omega_n, \mathbf{k}) & B(i\omega_n, \mathbf{k}) & 0 \\ C(i\omega_n, \mathbf{k}) & 0 & 0 & B(i\omega_n, \mathbf{k}) \end{pmatrix}, \quad (9)$$

where

$$\begin{aligned} A(i\omega_n, \mathbf{k}) &= \frac{i\omega_n + \zeta_{\mathbf{k}-\mathbf{q}/2}}{(i\omega_n - \zeta_{\mathbf{k}+\mathbf{q}/2})(i\omega_n + \zeta_{\mathbf{k}-\mathbf{q}/2}) - |\Delta|^2} \\ B(i\omega_n, \mathbf{k}) &= \frac{i\omega_n - \zeta_{\mathbf{k}+\mathbf{q}/2}}{(i\omega_n - \zeta_{\mathbf{k}+\mathbf{q}/2})(i\omega_n + \zeta_{\mathbf{k}-\mathbf{q}/2}) - |\Delta|^2} \\ C(i\omega_n, \mathbf{k}) &= \frac{|\Delta|}{(i\omega_n - \zeta_{\mathbf{k}+\mathbf{q}/2})(i\omega_n + \zeta_{\mathbf{k}-\mathbf{q}/2}) - |\Delta|^2}. \end{aligned} \quad (10)$$

Here, $\omega_n = (2n + 1)\pi k_B T$ are the Matsubara frequencies with n being integer and T representing the temperature. From this Green function, one obtains the particle density matrix at the equilibrium state,

$$\rho_e^c(\mathbf{k}) = \begin{pmatrix} \mathcal{A}(\mathbf{k}) & 0 & 0 & \mathcal{C}(\mathbf{k}) \\ 0 & \mathcal{A}(\mathbf{k}) & -\mathcal{C}(\mathbf{k}) & 0 \\ 0 & -\mathcal{C}(\mathbf{k}) & \mathcal{B}(\mathbf{k}) & 0 \\ \mathcal{C}(\mathbf{k}) & 0 & 0 & \mathcal{B}(\mathbf{k}) \end{pmatrix}, \quad (11)$$

whose diagonal elements denote the electron and hole distributions, and the off-diagonal elements represent the anomalous correlations due to the superconducting order parameter.

In Eq. (11),

$$\mathcal{A}(\mathbf{k}) \equiv \langle a_{\mathbf{k}+\frac{\mathbf{q}}{2}\uparrow}^{\dagger} a_{\mathbf{k}+\frac{\mathbf{q}}{2}\uparrow} \rangle = u_{\mathbf{k}}^2 f(E_{\mathbf{k}}^+) + v_{\mathbf{k}}^2 f(E_{\mathbf{k}}^-)$$

$$\mathcal{B}(\mathbf{k}) \equiv \langle a_{-\mathbf{k}+\frac{\mathbf{q}}{2}\uparrow} a_{-\mathbf{k}+\frac{\mathbf{q}}{2}\uparrow}^{\dagger} \rangle = v_{\mathbf{k}}^2 f(E_{\mathbf{k}}^+) + u_{\mathbf{k}}^2 f(E_{\mathbf{k}}^-)$$

$$\mathcal{C}(\mathbf{k}) \equiv \langle a_{-\mathbf{k}+\frac{\mathbf{q}}{2}\downarrow} a_{\mathbf{k}+\frac{\mathbf{q}}{2}\uparrow} \rangle = u_{\mathbf{k}}v_{\mathbf{k}}f(E_{\mathbf{k}}^+) - u_{\mathbf{k}}v_{\mathbf{k}}f(E_{\mathbf{k}}^-), \quad (12)$$

where $f(E_{\mathbf{k}}) = 1/\{\exp[E_{\mathbf{k}}/(k_B T)] + 1\}$ is the Fermi distribution function. For the quasiparticle, by a unitary transformation, the density matrix at the equilibrium state is

$$\begin{aligned} \rho_e^h(\mathbf{k}) &= U_{\mathbf{k}} \rho_e^c(\mathbf{k}) U_{\mathbf{k}}^{\dagger} \\ &= \text{diag}\{f(E_{\mathbf{k}}^+), f(E_{\mathbf{k}}^+), f(E_{\mathbf{k}}^-), f(E_{\mathbf{k}}^-)\}, \end{aligned} \quad (13)$$

in which only the diagonal elements exist, denoting the quasidelectron and quasihole distributions.

From the quasiparticle distribution at the equilibrium state, one specific feature arises due to the modification of the energy spectrum by the superconducting velocity [77,78,81–83]. It is noted that when $\mathbf{v}_s = 0$, $E_{\mathbf{k}}^+$ ($E_{\mathbf{k}}^-$) is always bigger (smaller) than zero. When $\mathbf{v}_s \neq 0$, it can be found that when $m^*v_s^2\mu/2 > |\Delta|^2$, there exist regions in which $E_{\mathbf{k}}^+ < 0$ and $E_{\mathbf{k}}^- > 0$ are satisfied. These regions are referred to as the blocking regions because they are occupied by the quasidelectrons even at zero temperature [81–83]. Specifically, the blocking region for the quasidelectron is written as

$$\begin{aligned} -\sqrt{\frac{m^*v_s^2\mu}{2} - |\Delta|^2} < \zeta_{\mathbf{k}} - \frac{m^*v_s^2}{8} < \sqrt{\frac{m^*v_s^2\mu}{2} - |\Delta|^2} \\ -1 \leq \cos \theta_{\mathbf{k}} < -\sqrt{\frac{[\zeta_{\mathbf{k}} + m^*v_s^2/8]^2 + |\Delta|^2}{m^*v_s^2/2[\zeta_{\mathbf{k}} + \mu]}}, \end{aligned} \quad (14)$$

with $\theta_{\mathbf{k}}$ being the angle between the momentum and superconducting velocity. Finally, it is addressed that in the Fulde-Ferrell-Larkin-Ovchinnikov (FFLO) state [81–83], the Zeeman-field-induced center-of-mass momentum of Cooper pairs plays similar role to the superconducting velocity here.

B. Numerical results

In this part, we present the numerical results for the properties of the quasiparticle state in GaAs QWs. All parameters including the band structure and material parameters used in our computation are listed in Table I [92,93]. In the table, n_e is the electron density, and P_0 represents the initial spin polarization.

1. Blocking region

We first analyze the energy spectrum of the quasidelectron [Eq. (1)]. It is assumed that the superconducting velocity is small, which influences the superconducting state in the

TABLE I. Parameters including the band structure and material parameters used in the computation [92,93].

m^*/m_0	0.067	n_e (cm ⁻²)	10 ¹¹
κ_0	12.9	γ_D (eV Å ³)	23.9
κ_{∞}	10.8	a (nm)	20
P_0	1%	T (K)	1

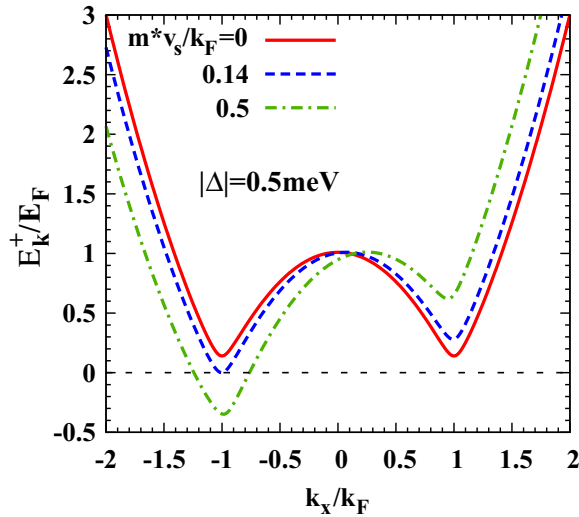


FIG. 3. Energy spectra of the quasielectron with different superconducting velocities $m^*v_s/k_F = 0$ (the red solid curve), 0.14 (the blue dashed curve) and 0.5 (the green chain curve). $|\Delta| = 0.5$ meV in the calculation. When $m^*v_s/k_F = 0$, the excitation energy is symmetric for $k_x > 0$ and $k_x < 0$. However, the finite superconducting velocity can cause the tilt of the energy spectrum. Specifically, when $m^*v_s/k_F \geq 0.14$, $E_{\mathbf{k}}^+ \leq 0$ can be realized.

s -wave superconductor marginally [77,78]. However, when $|\Delta| \ll |\Delta_S|$ here, it can efficiently tune the superconducting state in QWs. Without loss of generality, we assume that the superconducting velocity is along the \hat{x} direction. In Fig. 3, the k_x dependencies of the energy spectra of the quasielectron are plotted at different superconducting velocities. It can be seen from the figure that without the supercurrent (the red solid curve), the excitation energy is symmetric for $k_x > 0$ and $k_x < 0$. When there is finite superconducting velocity, the energy spectrum becomes tilted. Specifically, when $m^*v_s/k_F = 0.14$, $E_{\mathbf{k}}^+ = 0$ can be realized, which is represented by the blue dashed curve; when $m^*v_s/k_F > 0.14$, there exist regions with $E_{\mathbf{k}}^+ < 0$, as shown by the green chain curve when $m^*v_s/k_F = 0.5$. Here, k_F is the Fermi momentum of the electron.

When $E_{\mathbf{k}}^+ < 0$, the blocking region appears, which is determined by Eq. (14). When $v_s = 0.5k_F/m^*$, the quasielectron population at the equilibrium state is calculated [Eq. (13)], whose momentum dependence is plotted in Fig. 4(a). It can be seen from Fig. 4(a) that the blocking region is in the crescent shape, whose boundary constitutes the Fermi surface for the quasielectron. Furthermore, it can be seen that in the Fermi surface, its left and right boundaries are contributed by the electron- and holelike branches, respectively, in the shapes of arcs, referred to as Fermi arcs in the following. It is addressed that even though $|\Delta|$ is taken to the finite here, the basic pictures of the blocking region as well as the Fermi arcs remain the same as those revealed in Figs. 1 and 2.

Actually, the electron distribution in the particle space is also significantly influenced due to the superconducting velocity [Eq. (11)], whose Fermi surface is no longer a circle, as shown in Fig. 4(b). It can be seen from Fig. 4(b) that a crescent region at $k_x > 0$ (labeled by ‘‘A,’’ enclosed by

the dots) disappears and a new crescent region (labeled by ‘‘B’’) emerges at $k_x < 0$. The modification of the electron distribution inevitably influences the anomalous correlations when there exists a supercurrent. In the presence of the supercurrent, there exist the anomalous correlations between the electron states with momentum $\mathbf{k} + \mathbf{q}/2$ and $-\mathbf{k} + \mathbf{q}/2$, which can be calculated from $\mathcal{C}(\mathbf{k})$ in Eq. (12). This indicates that the Cooper pairs carry the center-of-mass momentum \mathbf{q} , driven by the supercurrent [77,78]. From the analysis of the electron distribution in Fig. 4(b), one finds that the absence of the crescent region at $k_x > 0$ makes the electrons in the newly arising crescent region at $k_x < 0$ unable to find their partners to constitute the Cooper pairs. Accordingly, there is no anomalous correlation for the electrons in the newly arising crescent region with $k_x < 0$ at zero temperature. The momentum dependence of the anomalous correlations without and with the superconducting velocity are explicitly shown in Figs. 4(c) and 4(d). It can be seen from those two figures that only the electrons around the Fermi surface can have efficient anomalous correlations. Specifically, in Fig. 4(c) without the supercurrent, all the electrons around the Fermi surface are paired. However, when $v_s = 0.5k_F/m^*$ in Fig. 4(d), the blocking region appears, in which the anomalous correlation is suppressed to be close to zero at low temperature. Accordingly, the residue regions with anomalous correlations are suppressed to be very small when the superconducting velocity is large. This shows that the superconducting velocity provides an efficient way to tune the Cooper pairing in the superconducting QWs.

2. Quasiparticle density

In this part, we show that the quasiparticle density in QWs can be efficiently tuned by the superconducting velocity. The quasiparticle density is calculated from the quasiparticle distributions in the presence of the superconducting velocity:

$$n^q = \sum_{\mathbf{k}} [f(E_{\mathbf{k}\uparrow}^+) + f(E_{\mathbf{k}\downarrow}^+)]. \quad (15)$$

In Fig. 5, the superconducting velocity dependence of the quasiparticle density with different order parameters $|\Delta| = 0.5, 0.3, 0.2,$ and 0.1 meV are plotted by the blue dashed, yellow dashed, red solid, and green chain curves. It is shown that with the increase of the superconducting velocity, the quasiparticle density first increases rapidly and then slowly, with the turning point corresponding to the appearance of the blocking region roughly. Specifically, with the increase of the quasiparticle density due to the superconducting velocity, the blocking region and the Fermi surface emerge. In this process, the system can experience the crossover between the nondegenerate and degenerate limits. Finally, it is noticed that when the superconducting velocity is large enough, the quasiparticle density is comparable to the one in the normal state.

3. Momentum current

In the presence of a finite superconducting velocity, the momentum current arises in the QW, which is calculated from

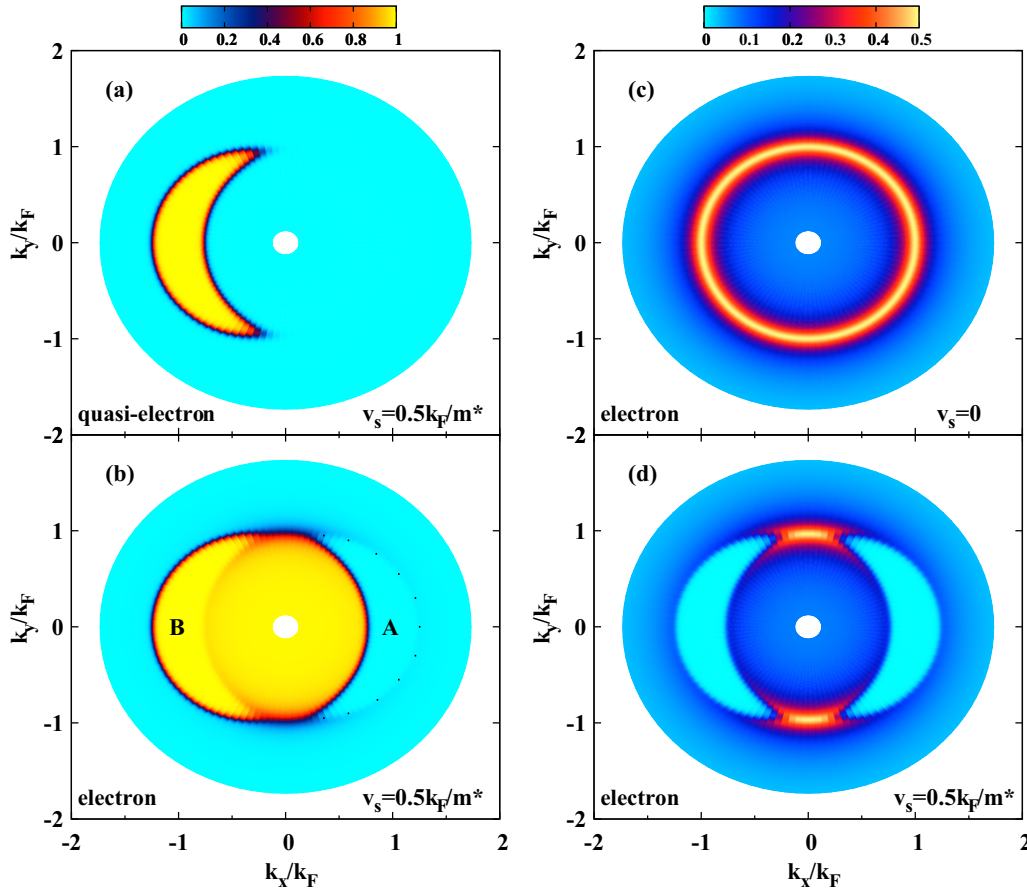


FIG. 4. Momentum dependencies of the quasielectron distribution [(a)], electron distribution [(b)], and anomalous correlations without [(c)] and with [(d)] the supercurrent. (a) is plotted in the quasiparticle space, whereas (b), (c), and (d) are shown in the particle space. In (a) and (b), $v_s = 0.5k_F/m^*$. $|\Delta| = 0.5$ meV in all the calculations. Specifically, in (a), the quasielectron distribution is addressed, in which the blocking region in the crescent shape arises, whose boundary constitutes the “Fermi surface.” In (b), for the electron distribution, it is observed that a crescent region when $k_x > 0$ (labeled by “A,” enclosed by the dots) disappears and a new crescent region (labeled by “B”) appears when $k_x < 0$. In (c), we show the anomalous correlation without the supercurrent, in which all the electrons around the Fermi surface are paired. Finally, in (d), the anomalous correlation with the supercurrent ($v_s = 0.5k_F/m^*$) is presented. It can be seen that compared to (c), the regions with efficient anomalous correlations are suppressed to be very small.

the equilibrium density matrix,

$$\mathbf{J} = \sum_{\mathbf{k}} \frac{1}{2} \text{Tr} \left\{ \tau_3 \left[U_{\mathbf{k}} \rho_e^h(\mathbf{k}) U_{\mathbf{k}}^\dagger + \frac{1}{2} (\tau_3 - 1) \right] \right. \\ \left. \times \text{diag} \left(\mathbf{k} + \frac{\mathbf{q}}{2}, \mathbf{k} + \frac{\mathbf{q}}{2}, -\mathbf{k} + \frac{\mathbf{q}}{2}, -\mathbf{k} + \frac{\mathbf{q}}{2} \right) \right\}. \quad (16)$$

Obviously, $\mathbf{J}_y = 0$ when $\mathbf{q} = q\hat{x}$. In Fig. 6, the superconducting-velocity dependencies of \mathbf{J}_x are plotted with different order parameters $|\Delta| = 0.5, 0.3$ and 0.2 meV. The unit for the momentum current is set to be $J_0 \equiv n_e k_F (k_B T / E_F)$ with E_F being the Fermi energy for the electron. It is shown that with the increase of the superconducting velocity, the momentum current first increases linearly and then decreases slowly, with the emergence of a peak. By defining the superconducting velocity corresponding to the peak of the current as the critical velocity, it can be seen that the critical velocity increases with the increase of the order parameter.

We start our analysis from the case with small superconducting velocity (i.e., before the appearance of the blocking region). With small superconducting velocity satisfying

$\mathbf{k} \cdot \mathbf{v}_s \ll \mathcal{E}_{\mathbf{k}}$, the quasiparticle distribution function can be expanded as a series of \mathbf{v}_s . By keeping \mathbf{v}_s to its linear order and considering $|\Delta| \gg k_B T$ here, from Eqs. (11) and (16), the momentum current is calculated to be

$$\mathbf{J}_x^a \approx m^* v_s \sum_{\mathbf{k}} \left\{ u_{\mathbf{k}}^2 f(\mathcal{E}_{\mathbf{k}}) + v_{\mathbf{k}}^2 [1 - f(\mathcal{E}_{\mathbf{k}})] \right\} \\ + \sum_{\mathbf{k}} k_x^2 v_s \frac{\partial f(\mathcal{E}_{\mathbf{k}})}{\partial \mathcal{E}_{\mathbf{k}}} \approx m^* v_s \sum_{\mathbf{k}} v_{\mathbf{k}}^2. \quad (17)$$

It is noted that $v_{\mathbf{k}}^2$ is just the distribution function of the Cooper pair condensate when $\mathbf{v}_s = 0$ (e.g., refer to Takahashi *et al.* [28,77,78]), and hence here the momentum current is mainly carried by the Cooper pairs. The results calculated from Eq. (17) when $|\Delta| = 0.5$ meV is plotted by the green chain curve in Fig. 6, which almost coincides with the blue dashed curve when \mathbf{v}_s is small. However, when the superconducting velocity is large, i.e., with the appearance of the blocking region, the current contributed from the quasiparticles becomes significant. Specifically, the quasielectron (quasihole) mainly populate with $k_x < 0$ ($k_x > 0$). Therefore, from Eq. (16), the

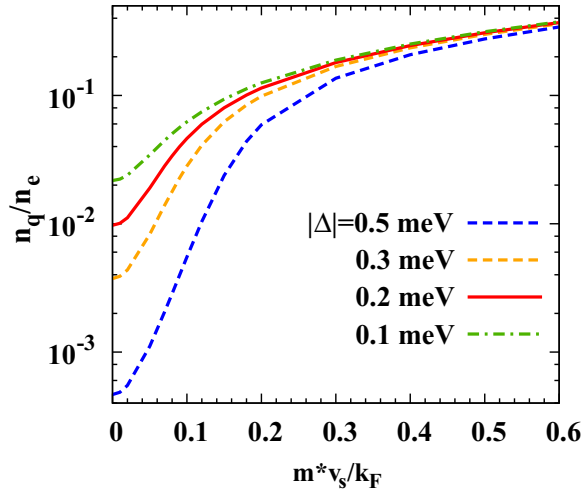


FIG. 5. Superconducting velocity dependence of the quasiparticle density with different order parameters $|\Delta| = 0.5$ meV (the blue dashed curve), 0.3 (the yellow dashed curve), 0.2 (the red solid curve), and 0.1 meV (the green chain curve). With the increase of the superconducting velocity, the quasiparticle density first increases rapidly and then slowly, with the turning point corresponding to the appearance of the blocking region approximately.

current contributed by the quasiparticles flows in the *opposite* direction to the one carried by the Cooper pairs. Accordingly, there exists the competition between the quasiparticles and Cooper pairs, leading to the critical velocity. Thus, the critical velocity can be estimated by $v_s^c \approx \sqrt{2}|\Delta|^2/(m^*\mu)$, which just corresponds to the appearance of the blocking region.

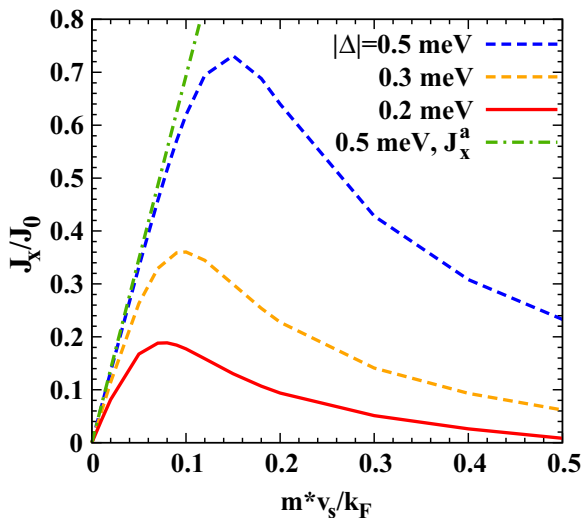


FIG. 6. Superconducting velocity dependence of the momentum current with different order parameters $|\Delta| = 0.5$ (the blue dashed curve), 0.3 (the yellow dashed curve), and 0.2 meV (the red solid curve). The unit for the momentum current is set to be $J_0 \equiv n_e k_F (k_B T / E_F)$. The green chain curve shows the results calculated from Eq. (17) when $|\Delta| = 0.5$ meV, which describes the behavior of momentum current with small superconducting velocity fairly well.

4. Role of momentum scattering on quasiparticle state

Finally, we address the role of the momentum scattering on the quasiparticle state. High mobility QWs can be realized and in this “clean” case, the tilted energy spectrum and Fermi arc are expected to be stable. Nevertheless, when there exists disorders, i.e., in the “dirty” case, the tilted energy spectrum and Fermi arc can be disrupted due to the momentum scattering, which is a phase-breaking effect. Here, we show that the tilted energy spectrum and Fermi arc for the quasiparticle in the QWs can be stabilized by the condensate, with the condition estimated as follows.

In the proximity effect, the Andreev reflection is the key mechanism when considering the single particle tunneling [94–96]. In the Andreev reflection from the superconducting metal to the QWs, the time for the tunneling electrons combining into the Cooper pairs is estimated by ξ/v_F , with ξ and v_F being the coherence length in the QWs and the Fermi velocity in the superconducting metal. When the combination time is smaller than the momentum scattering time, i.e., $\xi/v_F \lesssim \tau_p$, the momentum scattering is expected to have little influence on phase-breaking in the Andreev reflection. Here, the coherence length in the QWs is estimated by $\xi \approx v_S \hbar / |\Delta|$ with v_S being the Fermi velocity in the QWs [94–96]. One obtains $|\Delta| \gtrsim (v_S/v_F)(\hbar/\tau_p)$. Specifically, for $\tau_p \gtrsim 1$ ps and $v_S/v_F = 50$, one obtains $|\Delta| \gtrsim 0.01$ meV. Therefore, even when the order parameter in the QWs is extremely small, the superconducting phase is marginally influenced by the disorder because of the large Fermi velocity mismatch between the QWs and superconducting metal.

Once the Cooper pairs with finite momentum are created in the proximity effect, the impurity scattering cannot average their center-of-mass momentum to be zero. This is because there exists a source, i.e., the superconducting metal, to inject the Cooper pairs with definite momentum. It is noted that this is very different from the FFLO state in the *genuine* superconductor, in which the disorder can average the center-of-mass momentum of the Cooper pair and hence destroy the FFLO state [97,98]. Then in the presence of the superconducting velocity in the QWs, for the quasiparticle, the disorder in the QWs mainly causes the broadening of the energy spectrum due to the finite lifetime of the quasiparticle state. However, this broadening cannot destroy the tilted energy spectrum and Fermi arc, which are driven and stabilized by the condensate.

IV. QUASIPARTICLE SPIN RELAXATION

In this section, we study the quasiparticle spin relaxation in the superconducting GaAs (100) QWs. We first derive the KSBEs for the quasiparticle in the quasiparticle approximation [18,21,63–72], via the nonequilibrium Green function method with the generalized Kadanoff-Baym (GKB) ansatz [9,99,100] (Sec. IV A), and then show the numerical results for the SRTs without (Sec. IV B 1) and with the supercurrent (Sec. IV B 2).

A. KSBEs

1. Derivation with full Hamiltonian

With a small Fermi energy in the semiconductor QWs, the derivation of the KSBEs is based on the quasiparticle

approximation [18,21,63–72,99]. In the quasiparticle space, the contour-ordered nonequilibrium Green function is defined as [9,64,99]

$$G_{12} = -i \langle T_c \Psi_1 \Psi_2^\dagger \rangle = \begin{pmatrix} G_{12}^{++} & G_{12}^{+-} \\ G_{12}^{-+} & G_{12}^{--} \end{pmatrix}, \quad (18)$$

which is an 8×8 matrix. Here, $1 = (t_1, \mathbf{r}_1)$ represents the time-space point, T_c denotes the time contour, and $\Psi(t, \mathbf{r}) = (\alpha_\uparrow(t, \mathbf{r}), \alpha_\downarrow(t, \mathbf{r}), \alpha_\uparrow^\dagger(t, \mathbf{r}), \alpha_\downarrow^\dagger(t, \mathbf{r}))^T$ is the quasiparticle field operator. Specifically, $G_{12}^{++} = -i \langle T \Psi_1 \Psi_2^\dagger \rangle$, $G_{12}^{+-} \equiv G_{12}^< = i \langle \Psi_2^\dagger \Psi_1 \rangle$, $G_{12}^{-+} \equiv G_{12}^> = -i \langle \Psi_1 \Psi_2^\dagger \rangle$ and $G_{12}^{--} = -i \langle \tilde{T} \Psi_1 \Psi_2^\dagger \rangle$ with T and \tilde{T} representing the chronological ordering and anti-chronological ordering, respectively.

The contour-ordered Green function G_{12} satisfies the Gor'kov's equations [90,91]

$$\left[i \frac{\partial}{\partial t_1} - \vec{H}_0^q(\hat{\mathbf{k}}_1) \right] G_{12} = \delta(1-2) \tilde{\tau}_3 + \int_c d3 \tilde{\tau}_3 \Sigma_{13} G_{32}, \quad (19)$$

$$G_{12} \left[-i \frac{\partial}{\partial t_2} - \vec{H}_0^q(-\hat{\mathbf{k}}_2) \right] = \delta(1-2) \tilde{\tau}_3 + \int_c d3 \Sigma_{13} G_{32} \tilde{\tau}_3. \quad (20)$$

Here, $\tilde{\tau}_3 = \text{diag}(\mathbf{I}_{4 \times 4}, -\mathbf{I}_{4 \times 4})$, and Σ_{13} is the self-energy due to the quasiparticle-impurity interaction. Specifically, from Eqs. (19) and (20), one obtains the kinetic equations

$$\begin{aligned} & \int \frac{dE}{2\pi} e^{-iEt} \frac{\partial G^<(\mathbf{R}, T; \mathbf{k}, E)}{\partial T} + i \left[H_0^q, \int \frac{dE}{2\pi} e^{-iEt} G^<(\mathbf{R}, T; \mathbf{k}, E) \right] - \frac{1}{2} \left\{ \frac{\partial H_0^q}{\partial \mathbf{R}}, \int \frac{dE}{2\pi} e^{-iEt} \frac{\partial G^<(\mathbf{R}, T; \mathbf{k}, E)}{\partial \mathbf{k}} \right\} \\ & + \frac{1}{2} \left\{ \frac{\partial H_0^q}{\partial \mathbf{k}}, \int \frac{dE}{2\pi} e^{-iEt} \frac{\partial G^<(\mathbf{R}, T; \mathbf{k}, E)}{\partial \mathbf{R}} \right\} = -i \int_{-\infty}^{t_1} dt_3 [\Sigma^>(\mathbf{R}, \mathbf{k}; t_1, t_3) G^<(\mathbf{R}, \mathbf{k}; t_3, t_1) + G^<(\mathbf{R}, \mathbf{k}; t_1, t_3) \\ & \times \Sigma^>(\mathbf{R}, \mathbf{k}; t_3, t_1) - \Sigma^<(\mathbf{R}, \mathbf{k}; t_1, t_3) G^>(\mathbf{R}, \mathbf{k}; t_3, t_1) - G^>(\mathbf{R}, \mathbf{k}; t_1, t_3) \Sigma^<(\mathbf{R}, \mathbf{k}; t_3, t_1)]. \end{aligned} \quad (24)$$

Here, $[\cdot, \cdot]$ and $\{\cdot, \cdot\}$ represent the commutator and anticommutator, respectively; $\Sigma^<(\mathbf{R}, \mathbf{k}; t_1, t_3) = n_i \sum_{\mathbf{k}'} V_{\mathbf{k}'-\mathbf{k}}^q G^<(\mathbf{R}, \mathbf{k}'; t_1, t_3) V_{\mathbf{k}-\mathbf{k}'}$ with n_i standing for the impurity density.

In Eq. (24), the full BdG Hamiltonian $H_0^q(\mathbf{k})$ [Eq. (6)] is used, from which neither the detailed balance nor the quasiparticle number conservation are satisfied. This can be seen as follows. On one hand, the summation over \mathbf{k} on the right-hand side of Eq. (24) is not zero due to the matrix form of $V_{\mathbf{k}-\mathbf{k}'}$, which indicates the violation of detailed balance. On the other hand, from the second term in the left-hand side of Eq. (24), the off-diagonal 2×2 blocks in $H_0^q(\mathbf{k})$ can break the quasiparticle number conservation because of the precession between the quasidelectron and quasihole. This is not strange because in $H_0^q(\mathbf{k})$, the quasiparticle number operator does not commute with the BdG Hamiltonian (also the electron-impurity interaction Hamiltonian) because of the terms proportional to $\alpha \alpha^\dagger S^\dagger$ and $\alpha^\dagger \alpha^\dagger S$ [18,84–86]. Here, S and S^\dagger are the annihilation and creation operators for the Cooper pairs [18,84–86]. Specifically, these terms are related to the annihilation or creation of two quasiparticles to create or annihilate one Cooper pair [18,84–86].

Nevertheless, it suggests that when the process for the quasiparticle annihilation (creation) to (from) the Cooper pair

for $G_{12}^<$,

$$\left[i \frac{\partial}{\partial t_1} - \vec{H}_0^q(\hat{\mathbf{k}}_1) \right] G_{12}^< = \int d3 (\Sigma_{13}^R G_{32}^< + \Sigma_{13}^< G_{32}^A), \quad (21)$$

$$G_{12}^< \left[-i \frac{\partial}{\partial t_2} - \vec{H}_0^q(-\hat{\mathbf{k}}_2) \right] = \int d3 (G_{13}^R \Sigma_{32}^> + G_{13}^> \Sigma_{32}^A), \quad (22)$$

where “R” and “A” label the retarded and advanced Green functions [64–66,69,99].

By defining $(t, \mathbf{r}) = (t_1 - t_2, \mathbf{r}_1 - \mathbf{r}_2)$ and $(\mathbf{R}, T) = (t_1 + t_2, \mathbf{r}_1 + \mathbf{r}_2)/2$ and then taking the difference of Eqs. (21) and (22), one obtains

$$\begin{aligned} & i \partial_T G_{12}^< - \left[H_0^q(\hat{\mathbf{k}}_1) G_{12}^< - G_{12}^< H_0^q(-\hat{\mathbf{k}}_2) \right] \\ & = \int d3 (\Sigma_{13}^R G_{32}^< + \Sigma_{13}^< G_{32}^A - G_{13}^R \Sigma_{32}^> - G_{13}^> \Sigma_{32}^A). \end{aligned} \quad (23)$$

From Eq. (23), by using the gradient expansion, [99] the kinetic equation is derived for the Fourier component of $G_{12}^<$, i.e., $G^<(\mathbf{R}, T; \mathbf{k}, E) = \int dt d\mathbf{r} e^{iEt - i\mathbf{k}\cdot\mathbf{r}} G^<(\mathbf{R}, T; \mathbf{r}, t)$, which is written as

condensate is slow compared to the process under investigation, the part violating the quasiparticle number conservation in the full Hamiltonian can be neglected. This approximation has been well applied in the derivation of the quasiparticle kinetic equation (e.g., Refs. [18,57,67]). Fortunately, once the Hamiltonian violating the quasiparticle number conservation is neglected, the detailed balance is automatically satisfied. We address that this assumption is reasonable for the *weak* SOC and low impurity density in this investigation.

The violation of the detailed balance and quasiparticle number conservation can also be understood from the mathematical point of view. It is noted that the Gor'kov space spanned by the “electron” and “hole” bands is larger than the real physical space. For linear operations on the Green function, no consequence will occur. However, for nonlinear operations, unphysical consequence may appear.

2. KSBES with detailed balance and quasiparticle number conservation satisfied

From the above analysis, to obtain a self-consistent kinetic equation, we neglect the off-diagonal 2×2 blocks in both the BdG Hamiltonian [Eq. (6)] and quasiparticle-impurity interaction Hamiltonian [Eq. (7)]. To further derive the scattering term, the GKB ansatz and Markovian approximation are

used [9,99,100]. Specifically, in the GKB ansatz [9,99,100],

$$G^{\lessgtr}(\mathbf{R}, \mathbf{k}; t_1, t_2) = \mp [G^R(\mathbf{R}, \mathbf{k}; t_1, t_2) \rho^{\lessgtr}(\mathbf{R}, \mathbf{k}; t_2) - \rho^{\lessgtr}(\mathbf{R}, \mathbf{k}; t_1) G^A(\mathbf{R}, \mathbf{k}; t_1, t_2)], \quad (25)$$

where $\rho^{\lessgtr}(\mathbf{R}, \mathbf{k}; t) = -i \int dE / (2\pi) G^{\lessgtr}(\mathbf{R}, \mathbf{k}; t, E)$. In Eq. (25), $G^R(\mathbf{R}, \mathbf{k}; t_1, t_2)$ and $G^A(\mathbf{R}, \mathbf{k}; t_1, t_2)$ are further approximated by their free equilibrium forms, written as

$$G^R(\mathbf{k}; t_1, t_2) \approx -i\theta(t_1 - t_2) \exp[-i(t_1 - t_2)H'_0(\mathbf{k})], \quad (26)$$

$$G^A(\mathbf{k}; t_1, t_2) \approx i\theta(t_2 - t_1) \exp[-i(t_1 - t_2)H'_0(\mathbf{k})]. \quad (27)$$

Here, $\theta(x)$ is the Heaviside step function, and $H'_0(\mathbf{k})$ does not include the off-diagonal 2×2 blocks. In the Markovian approximation [9,99],

$$\rho^{\lessgtr}(\mathbf{R}, \mathbf{k}; t_3) = \exp[iH'_0(\mathbf{k})(t_1 - t_3)] \rho(\mathbf{R}, \mathbf{k}; t_1) \times \exp[-iH'_0(\mathbf{k})(t_1 - t_3)]. \quad (28)$$

Furthermore, due to the small SOC, its contribution to the second and third terms in the left and right-hand sides of Eq. (24) can be neglected [9].

Finally, by taking $t_1 \rightarrow t_2$, i.e., $t \rightarrow 0$, from the E -integrated Green function, one obtains the KSBEs of the quasiparticle,

$$\begin{aligned} \frac{\partial \rho_{\mathbf{k}}^h}{\partial T} + \left(\frac{\mathbf{v}_s}{2} + \frac{\epsilon_{\mathbf{k}}}{\mathcal{E}_{\mathbf{k}}} \frac{\mathbf{k}}{m^*} \tau_3 \right) \cdot \frac{\partial \rho_{\mathbf{k}}^h}{\partial \mathbf{R}} + \frac{\epsilon_{\mathbf{k}}}{\mathcal{E}_{\mathbf{k}}} \left[-\frac{\partial \mu(\mathbf{R})}{\partial \mathbf{R}} \right] \tau_3 \frac{\partial \rho_{\mathbf{k}}^h}{\partial \mathbf{k}} \\ + i \left[\begin{pmatrix} h_{\text{soc}}^e(\mathbf{k}) & 0 \\ 0 & h_{\text{soc}}^h(\mathbf{k}) \end{pmatrix}, \rho_{\mathbf{k}}^h \right] = -2\pi n_i \sum_{\mathbf{k}'} |V_{\mathbf{k}-\mathbf{k}'}^{\text{eff}}|^2 \\ \times \left[\delta(E_{\mathbf{k}'}^+ - E_{\mathbf{k}}^+) \frac{1 + \tau_3}{2} (\rho_{\mathbf{k}'}^h - \rho_{\mathbf{k}}^h) + \delta(E_{\mathbf{k}'}^- - E_{\mathbf{k}}^-) \right. \\ \left. \times \frac{1 - \tau_3}{2} (\rho_{\mathbf{k}'}^h - \rho_{\mathbf{k}}^h) \right], \end{aligned} \quad (29)$$

where

$$|V_{\mathbf{k}-\mathbf{k}'}^{\text{eff}}|^2 = |V_{\mathbf{k}-\mathbf{k}'}|^2 (u_{\mathbf{k}} u_{\mathbf{k}'} - v_{\mathbf{k}} v_{\mathbf{k}'}')^2, \quad (30)$$

$$h_{\text{soc}}^e(\mathbf{k}) = \begin{pmatrix} 0 & \frac{\epsilon_{\mathbf{k}}}{\mathcal{E}_{\mathbf{k}}} h_{\mathbf{k}} + h_{\frac{q}{2}} \\ \frac{\epsilon_{\mathbf{k}}}{\mathcal{E}_{\mathbf{k}}} h_{\mathbf{k}}^* + h_{\frac{q}{2}}^* & 0 \end{pmatrix}, \quad (31)$$

$$h_{\text{soc}}^h(\mathbf{k}) = \begin{pmatrix} 0 & \frac{\epsilon_{\mathbf{k}}}{\mathcal{E}_{\mathbf{k}}} h_{\mathbf{k}}^* - h_{\frac{q}{2}}^* \\ \frac{\epsilon_{\mathbf{k}}}{\mathcal{E}_{\mathbf{k}}} h_{\mathbf{k}} - h_{\frac{q}{2}} & 0 \end{pmatrix}. \quad (32)$$

In this investigation at extremely low temperature, the quasiparticle-quasiparticle and quasiparticle-phonon interactions are inefficient and hence only the quasiparticle-impurity scattering is presented here. One notes that when the SOC and \mathbf{v}_s are taken to be zero, Eq. (29) can recover the traditional Boltzmannlike equation for the quasiparticle [18,28,57,63,67]. Moreover, when $|\Delta|$ and \mathbf{v}_s are taken to be zero, Eq. (29) can also recover the conventional KSBEs for electrons [9].

In Eq. (29), the second, third, and fourth terms correspond to the diffusion, drift, and coherence terms, respectively. Their physical origins are clear from the point of view that the quasiparticle state is the combination of the electron and hole ones [Eq. (5)] [18,20,25,28,67]. Specifically, for the diffusion

term, one notes that the group velocities for the quasielectron and quasihole are $\frac{v_s}{2} + \frac{\epsilon_{\mathbf{k}}}{\mathcal{E}_{\mathbf{k}}} \frac{\mathbf{k}}{m^*}$ and $\frac{v_s}{2} - \frac{\epsilon_{\mathbf{k}}}{\mathcal{E}_{\mathbf{k}}} \frac{\mathbf{k}}{m^*}$, respectively, which correspond to the quasiparticle velocities in Eq. (29). For the drift term, it can be seen that the charges for the quasielectron and quasihole are $-|e|(u_{\mathbf{k}}^2 - v_{\mathbf{k}}^2) = -|e|\epsilon_{\mathbf{k}}/\mathcal{E}_{\mathbf{k}}$ and $|e|\epsilon_{\mathbf{k}}/\mathcal{E}_{\mathbf{k}}$, respectively, which are just responsible for the electrical force experienced by the quasiparticle under the electrical field. Finally, for the coherence term, the SOC experienced by the quasielectron [Eq. (32)] is the combination of the ones experienced by the electron and hole, which can be calculated from

$$h_{\text{soc}}^e(\mathbf{k}) = u_{\mathbf{k}}^2 \begin{pmatrix} 0 & h_{\mathbf{k}+\frac{q}{2}} \\ h_{\mathbf{k}+\frac{q}{2}}^* & 0 \end{pmatrix} + v_{\mathbf{k}}^2 \begin{pmatrix} 0 & -h_{\mathbf{k}-\frac{q}{2}} \\ -h_{\mathbf{k}-\frac{q}{2}}^* & 0 \end{pmatrix}. \quad (33)$$

B. Numerical results

In this part, we study the quasiparticle spin relaxation in the spatially homogeneous system. By numerically solving the KSBEs [Eq. (29)], one obtains the SRT from the time evolution of the spin polarization

$$\mathbf{S}(t) = \sum_{\mathbf{k}} \frac{1}{4n_q} \text{Tr} \left\{ \tau_3 \left[\rho_{\mathbf{k}}^h(t) + \frac{1}{2}(\tau_3 - 1) \text{diag}(\boldsymbol{\sigma}, -\boldsymbol{\sigma}) \right] \right\}, \quad (34)$$

where $\boldsymbol{\sigma}$ are the Pauli matrices. Here, we focus on the situation that the initial spin polarization of the quasiparticle is along the \hat{z} direction, corresponding to the spin imbalance, which can be realized by the spin injection with small charge imbalance [19,20,22–29,31,32]. Accordingly, the initial density matrix for the quasiparticle is written as

$$\rho_{\mathbf{k}}^h(t=0) = \text{diag}[f(E_{\mathbf{k}\uparrow}^+), f(E_{\mathbf{k}\downarrow}^+), f(E_{\mathbf{k}\uparrow}^-), f(E_{\mathbf{k}\downarrow}^-)], \quad (35)$$

where $f(E_{\mathbf{k}\uparrow}^{\pm}) = f(E_{\mathbf{k}}^{\pm} + \mu_{\uparrow}^q)$ and $f(E_{\mathbf{k}\downarrow}^{\pm}) = f(E_{\mathbf{k}}^{\pm} + \mu_{\downarrow}^q)$. Here, μ_{\uparrow}^q and μ_{\downarrow}^q are determined by the density of quasielectrons with spin-up n_{\uparrow}^q and spin-down n_{\downarrow}^q , i.e.,

$$n_{\uparrow, \downarrow}^q = \sum_{\mathbf{k}} f(E_{\mathbf{k}\uparrow, \downarrow}^+) = \sum_{\mathbf{k}} f(E_{\mathbf{k}}^+ + \mu_{\uparrow, \downarrow}^q). \quad (36)$$

The parameters for the computation are listed in Table I.

1. Quasiparticle spin relaxation without a supercurrent

In this part, we analyze the quasiparticle spin relaxation without the supercurrent, i.e., $\mathbf{v}_s = 0$, and reveal the influence of the magnitude of the order parameter on the quasiparticle spin relaxation. When $|\Delta| = 0$, the system returns to the normal situation with the Rashba-like SOC, which has been well studied in GaAs (100) QWs [9]. In Fig. 7, it is shown that when $n_i \lesssim 0.05n_e$ ($n_i \gtrsim 0.05n_e$), the system lies in the weak- (strong) scattering regime with $\tau_s \propto \tau_{\mathbf{k}}^N$ [$\tau_s \propto (\tau_{\mathbf{k}}^N)^{-1}$]. Here, $\tau_{\mathbf{k}}^N$ is the momentum relaxation time in the normal state. When $|\Delta|$ varies from 0.1 to 0.5 meV, the SRTs are enhanced in both the weak and strong-scattering regimes. However, the boundary between the weak- and strong-scattering regimes is unchanged. This can be understood from the following analytical analysis.

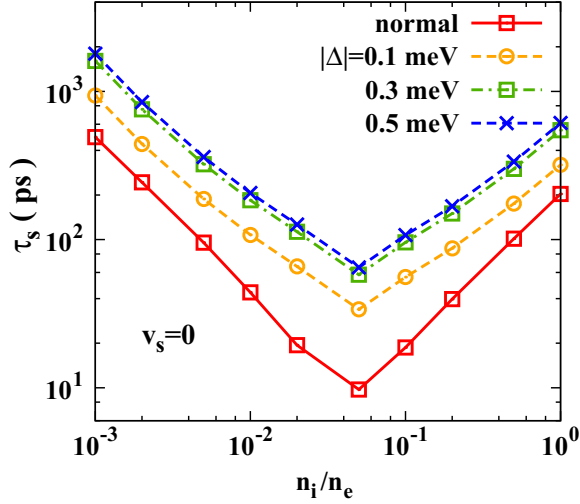


FIG. 7. Impurity density dependence of the quasiparticle SRTs without the supercurrent when $|\Delta| = 0$ (normal state, the red solid curve with squares), 0.1 (the yellow dashed curve with circles), 0.3 (the green chain curve with squares), and 0.5 meV (the blue dashed curve with crosses). No matter in the weak- or strong-scattering regime, the SRTs are enhanced in the superconducting state compared to the normal one. However, the boundary between the weak- and strong-scattering regimes is unchanged with the variation of the order parameter magnitudes.

From Eq. (29), one can see that when $v_s = 0$, both the SOC and momentum scattering for the quasiparticle are modified by the order parameter. Specifically, from the coherent term [the fourth term in Eq. (29)], one observes that when $v_s = 0$, the SOC is modified to be

$$h_{\text{soc}}^S(\mathbf{k}) = (\epsilon_{\mathbf{k}}/\mathcal{E}_{\mathbf{k}})h_{\text{soc}}^N(\mathbf{k}), \quad (37)$$

where $h_{\text{soc}}^N(\mathbf{k})$ is the normal-state SOC in GaAs (100) QW. Accordingly, due to the factor $\epsilon_{\mathbf{k}}/\mathcal{E}_{\mathbf{k}}$ in Eq. (37), the SOC is exactly zero when $|\mathbf{k}| = k_F$ and efficiently suppressed for the quasiparticles with momentum around k_F . For the scattering term, new features arise due to the modifications of the quasiparticle-impurity interaction potential [Eq. (30)] and the DOS. In the quasiparticle-impurity potential [Eq. (30)], the coherent factor $(u_{\mathbf{k}}u_{\mathbf{k}'} - v_{\mathbf{k}}v_{\mathbf{k}'})^2$ arises [18,67], which equals to $(\epsilon_{\mathbf{k}}/\mathcal{E}_{\mathbf{k}})^2$ because in the elastic scattering, the branch mixing is forbidden [36,37] and hence $|\mathbf{k}'| = |\mathbf{k}|$. Whereas the DOS is modified to be $(\mathcal{E}_{\mathbf{k}}/|\epsilon_{\mathbf{k}}|)N_0(\mathbf{k})$ with $N_0(\mathbf{k})$ being the DOS in the normal state. Accordingly, compared to the normal state, a new prefactor $|\epsilon_{\mathbf{k}}/\mathcal{E}_{\mathbf{k}}|$ arises in the scattering term for the superconducting state, which is also exactly zero when $|\mathbf{k}| = |\mathbf{k}'| = k_F$. Consequently, the momentum scattering time in the superconducting state becomes [18,21,84]

$$\tau_{\mathbf{k}}^S = (\mathcal{E}_{\mathbf{k}}/|\epsilon_{\mathbf{k}}|)\tau_{\mathbf{k}}^N. \quad (38)$$

Because at low temperature, the quasiparticles mainly populate around the states with momentum $|\mathbf{k}| = k_F$, the momentum scattering is efficiently suppressed in the superconducting state.

Obviously, from Eqs. (37) and (38), $|h_{\text{soc}}^S(\mathbf{k})|\tau_{\mathbf{k}}^S = |h_{\text{soc}}^N(\mathbf{k})|\tau_{\mathbf{k}}^N$, and hence the boundary between the weak- and strong scattering regimes remains unchanged when the system

enters to the superconducting state. Then by solving the KSBEs analytically, one obtains the SRTs in both the strong- and weak-scattering regimes [9,101,102]. Specifically, in the strong scattering limit with $\Omega_{\mathbf{k}}^S\tau_{\mathbf{k}}^S \ll 1$, $S_{\mathbf{k}}^z(t) \approx P_0 \exp[-4(\Omega_{\mathbf{k}}^S)^2\tau_{\mathbf{k}}^S t]$. Here,

$$\Omega_{\mathbf{k}}^S = (\alpha k)(\epsilon_{\mathbf{k}}/\mathcal{E}_{\mathbf{k}}) = \Omega_{\mathbf{k}}^N(\epsilon_{\mathbf{k}}/\mathcal{E}_{\mathbf{k}}) \quad (39)$$

is the precession frequency due to the SOC, and

$$\frac{1}{\tau_{\mathbf{k}}^S} = \frac{n_i m^*}{2\pi} \frac{\epsilon_{\mathbf{k}}}{\mathcal{E}_{\mathbf{k}}} \int d\theta_{\mathbf{k}-\mathbf{k}'} |V_{\mathbf{k}-\mathbf{k}'}|^2 (1 - \cos \theta_{\mathbf{k}-\mathbf{k}'}). \quad (40)$$

In the weak-scattering limit with $\Omega_{\mathbf{k}}^S\tau_{\mathbf{k}}^S \gg 1$, $S_{\mathbf{k}}^z(t) \approx P_0 \exp[-t/(2\tau_{\mathbf{k}}^S)] \cos(2\Omega_{\mathbf{k}}^S t)$. On one hand, the momentum scattering opens a spin relaxation channel due to the factor $\exp[-t/(2\tau_{\mathbf{k}}^S)]$; on the other hand, the factor $\cos(2\Omega_{\mathbf{k}}^S t)$ can cause the free induction decay due to different precession frequency with different momentum, which is suppressed in the degenerate regime [9,101,102]. Accordingly, the SRT for the quasiparticle with momentum \mathbf{k} reads

$$\tau_s^S(\mathbf{k}) \approx \begin{cases} [4(\Omega_{\mathbf{k}}^S)^2\tau_{\mathbf{k}}^S]^{-1}, & \Omega_{\mathbf{k}}^S\tau_{\mathbf{k}}^S \ll 1; \\ 2\tau_{\mathbf{k}}^S, & \Omega_{\mathbf{k}}^S\tau_{\mathbf{k}}^S \gg 1; \end{cases} \quad (41)$$

$$= (\mathcal{E}_{\mathbf{k}}/|\epsilon_{\mathbf{k}}|)\tau_s^N(\mathbf{k}), \quad (42)$$

with $\tau_s^N(\mathbf{k})$ being the SRT in the normal state. Due to the factor $\mathcal{E}_{\mathbf{k}}/|\epsilon_{\mathbf{k}}|$ in Eq. (42), no matter in the strong- or weak-scattering regime, the SRT for the quasiparticle with the momentum around k_F is *enhanced* compared to the normal one.

Finally, based on Eq. (42), we calculate the total SRT of the quasiparticle, written as [9,102]

$$\frac{1}{\tau_s} = \frac{\sum_{\mathbf{k}} \frac{1}{\tau_s^N(\mathbf{k})} \frac{|\epsilon_{\mathbf{k}}|}{\mathcal{E}_{\mathbf{k}}} [f(E_{\mathbf{k}\uparrow}) - f(E_{\mathbf{k}\downarrow})]}{\sum_{\mathbf{k}} [f(E_{\mathbf{k}\uparrow}) - f(E_{\mathbf{k}\downarrow})]}. \quad (43)$$

With the small spin polarization, the spin polarization is limited to the region around the Fermi surface, and hence in Eq. (43), $\tau_s^N(\mathbf{k}) \approx \tau_s^N(\mathbf{k}_F)$. Accordingly, from Eq. (43), one obtains

$$\frac{1}{\tau_s} \approx \frac{1}{\tau_s^N} \frac{1}{P_0 n_q} \frac{m^*}{2\pi} (\mu_{\uparrow}^q - \mu_{\downarrow}^q) [f(\sqrt{\mu^2 + |\Delta|^2}) - 2f(|\Delta|)]. \quad (44)$$

Furthermore, when $\mu \gg |\Delta|$ and $\mu_{\uparrow}^q \approx -\mu_{\downarrow}^q \equiv \delta\mu$ due to the small spin polarization, one obtains

$$\frac{1}{\tau_s} \approx \frac{1}{\tau_s^N} \frac{1}{P_0 n_q} \frac{2m^*}{\pi} |\delta\mu| f(|\Delta|) = Q \frac{1}{\tau_s^N}, \quad (45)$$

with $Q \equiv \frac{1}{P_0 n_q} \frac{2m^*}{\pi} |\delta\mu| f(|\Delta|)$. Here, with $|\Delta| = 0.1, 0.3$ and 0.5 meV, $1/Q$ is calculated to be 1.7, 2.7, and 3.3, in good agreement with the numerical results. From Eq. (45), this shows that due to the order parameter, the SRT can be enhanced by several times and increases with the increase of the order parameter. Finally, it is addressed that we also consider the influence of the *inelastic* quasiparticle-quasiparticle scattering on the quasiparticle spin relaxation, which is proven to be inefficient even with the low impurity density $n_i = 10^{-3}n_e$ [103].

2. Quasiparticle spin relaxation with a supercurrent

In this part, we consider the influence of the supercurrent or superconducting velocity on the quasiparticle spin relaxation

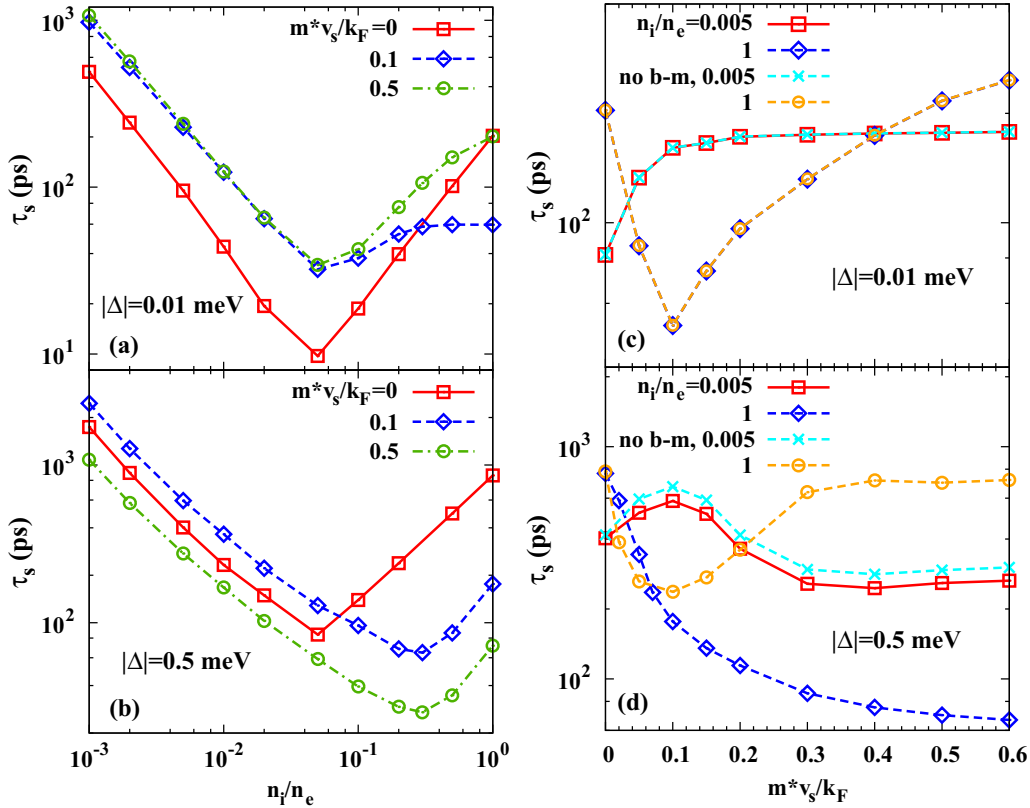


FIG. 8. Impurity density [(a) and (b)] and superconducting velocity [(c) and (d)] dependencies of the SRTs. In (a) and (c) [(b) and (d)], $|\Delta| = 0.01$ (0.5) meV. Specifically, in (a) and (b), the SRTs are plotted with different superconducting velocities $v_s = 0$ (the red solid curve with squares), $0.1k_F/m^*$ (the blue dashed curve with diamonds) and $0.5k_F/m^*$ (the green chain curve with circles). In (c) and (d), the SRTs are presented with different impurity densities $n_i/n_e = 0.005$ (the red solid curve with squares) and 1 (the blue dashed curve with squares). Finally, with the branch-mixing scattering removed, in (c) and (d), the SRTs are shown by the cyan (yellow) dashed curve with crosses (circles) when $n_i/n_e = 0.005$ (1).

with small and large order parameters $|\Delta| = 0.01$ and 0.5 meV, respectively. The superconducting velocity can cause the tilt of the quasiparticle energy spectrum and hence modifies the quasiparticle distribution (refer to Sec. III B 1), which is expected to cause rich physics in the quasiparticle spin relaxation. It is assumed that the condensation process associated with the annihilation of the quasidelectron and quasihole is slow compared to the spin relaxation rate. Here, we first describe the rich phenomenon from the impurity density and superconducting velocity dependencies of the quasiparticle SRTs.

Specifically, in Figs. 8(a) and 8(b), the impurity density dependencies of the SRTs are plotted with different superconducting velocities $v_s = 0$ (the red solid curve with squares), $0.1k_F/m^*$ (the blue dashed curve with diamonds) and $0.5k_F/m^*$ (the green chain curve with circles). In Fig. 8(a), with an extremely small order parameter $|\Delta| = 0.01$ meV, it can be seen that in the weak- (strong) scattering limit, the SRT can be enhanced (suppressed) by the superconducting velocity when $v_s \lesssim 0.5k_F/m^*$. Moreover, with the increase of the superconducting velocity, the boundary between the weak- and strong-scattering regimes remains unchanged. Anomalously, when the system enters into the strong-scattering regime, for $v_s \gtrsim 0.1k_F/m^*$, the SRT becomes *insensitive* to the

momentum scattering. However, when the order parameter is large enough with $|\Delta| \gtrsim 0.1$ meV, the behaviors of the SRT become different. Specifically, it can be seen from Fig. 8(b) that when $|\Delta| = 0.5$ meV, in the weak- (strong) scattering regime, the SRT can be either enhanced or suppressed (suppressed) by the superconducting velocity. In particular, for the superconducting velocity $v_s = 0.1k_F/m^*$, the boundary between the weak- and strong-scattering regimes is shifted, which arises at the larger impurity density and remains unchanged with the further increase of the superconducting velocity (e.g., $v_s = 0.5k_F/m^*$).

To see the role of the superconducting velocity on the quasiparticle spin relaxation more clearly, we further calculate the superconducting velocity dependencies of the SRTs with different impurity densities, shown in Figs. 8(c) and 8(d) at low and high impurity densities with $|\Delta| = 0.01$ and 0.5 meV. Specifically, in Fig. 8(c), one finds that when the order parameter is extremely small ($|\Delta| = 0.01$ meV), with the increase of the superconducting velocity, in the weak scattering regime with $n_i/n_e = 0.005$, the SRT first increases and then becomes insensitive to the superconducting velocity; whereas in the strong-scattering regime, the SRT first decreases rapidly and then increases. However, when the order parameter becomes larger (with $|\Delta| \gtrsim 0.1$ meV),

the response of the SRTs to the superconducting velocity also becomes very different. Specifically, it can be seen from Fig. 8(d) that when $|\Delta| = 0.5$ meV, with the increase of the superconducting velocity, the SRT in the weak-scattering regime ($n_i/n_e = 0.005$) first increases, then decreases and finally becomes insensitive to the superconducting velocity; whereas in the strong-scattering regime ($n_i/n_e = 1$), the SRT decreases monotonically.

Before a detailed explanation for the rich behaviors of the quasiparticle spin relaxation in the impurity density and superconducting velocity dependencies, we first address two important influences of the superconducting velocity on the quasiparticle state. On one hand, when a supercurrent exists, as addressed in Sec. III B 1, the quasiparticle energy spectrum is tilted by the superconducting velocity, and hence a blocking region can appear. Around the blocking region, the quasiparticle Fermi surface emerges, which consists of the electron- and holelike Fermi arcs (refer to Figs. 1 and 2). On the other hand, only when $|\Delta| \gtrsim 0.1$ meV, due to the superconducting velocity, the branch-mixing scattering [36,37] can be *efficiently* triggered due to the tilt of the energy spectrum (refer to Fig. 2). When $|\Delta| \rightarrow 0$, the branch-mixing scattering is forbidden because the coherence prefactor ($\approx \epsilon_{\mathbf{k}}/|\epsilon_{\mathbf{k}}| + \epsilon_{\mathbf{k}'}/|\epsilon_{\mathbf{k}'}|$) tends to zero in the momentum scattering [Eq. (30)].

a. Quasiparticle spin relaxation in a Fermi arc. We first analyze the quasiparticle spin relaxation with extremely small order parameters ($|\Delta| \ll 0.1$ meV). As addressed above, the branch-mixing scattering for the quasiparticle is forbidden, indicating that the electron- and holelike Fermi arcs are independent when the condensation process is slow enough. When $v_s \gtrsim 0.1k_F/m^*$, the quasiparticle distribution enters into the degenerate regime (refer to Fig. 5), and the thermal excitations of the quasiparticles happen around the Fermi arcs. In this situation, the quasiparticle spin relaxation can be simply understood by only analyzing the Fermi arc. Specifically, the angular average of the effective magnetic field in one Fermi arc, i.e., $\langle \Omega_{\mathbf{k}} \rangle_a$, is not zero. By writing the effective magnetic field as $\Omega_{\mathbf{k}} = (\Omega_{\mathbf{k}} - \langle \Omega_{\mathbf{k}} \rangle_a) + \langle \Omega_{\mathbf{k}} \rangle_a \equiv \Omega_{\mathbf{k}}^{\text{eff}} + \langle \Omega_{\mathbf{k}} \rangle_a$, one finds that around one Fermi arc, $\Omega_{\mathbf{k}}^{\text{eff}}$ plays the role of the effective magnetic field (inhomogeneous broadening [9,87]) and $\langle \Omega_{\mathbf{k}} \rangle_a$ acts as an effective Zeeman field. Specifically, at low temperature, the effective Zeeman field can cause the spin oscillations even in the strong-scattering regime (refer to Appendix).

Moreover, when $|\langle \Omega_{\mathbf{k}} \rangle_a|$ is comparable to $|\Omega_{\mathbf{k}}^{\text{eff}}|$, $\langle \Omega_{\mathbf{k}} \rangle_a$ plays marginal role on the spin relaxation, whereas $\Omega_{\mathbf{k}}^{\text{eff}}$ leads to the spin relaxation [6,9,104]. In particular, one finds that the magnitude of $\Omega_{\mathbf{k}}^{\text{eff}}$ *strongly* depends on the direction of the momentum. Accordingly, around one Fermi arc, the variation of momentum direction can cause the variations of both the direction and magnitude of the effective magnetic field, acting as the angle-dependent and modular-dependent inhomogeneous broadenings, respectively. In this situation, even due to the elastic scattering, the module-dependent inhomogeneous broadening is triggered [102], which is enhanced by the momentum scattering. Nevertheless, the motional narrowing effect can suppress the spin relaxation in the strong-scattering regime [40]. Thus the competition of the two trends leads to the insensitiveness of momentum scattering dependence of

the SRT in the strong-scattering regime. The above features for the spin relaxation in the strong-scattering regime actually provide a method for experimentally verifying the existence of the Fermi arc.

The Fermi arc structure also influences the quasiparticle spin relaxation in the weak-scattering regime. By assuming that the proportions of the spin polarization carried by the electron- and holelike branches are P_e and $1 - P_e$, respectively. Then, due to the separations of the electronlike (holelike) Fermi arc, the angular-averaged effective magnetic field magnitude is estimated to be $\langle |\Omega_{\mathbf{k}}^{\text{eff}}| \rangle_a \approx P_e |\Omega_{\mathbf{k}}| [(1 - P_e) |\Omega_{\mathbf{k}}|]$, and the momentum scattering time becomes $\tau_{\mathbf{k}}' \approx \tau_{\mathbf{k}}^N / P_e [\tau_{\mathbf{k}}^N / (1 - P_e)]$. Obviously, $\langle |\Omega_{\mathbf{k}}^{\text{eff}}| \rangle_a \tau_{\mathbf{k}}' \approx |\Omega_{\mathbf{k}}| \tau_{\mathbf{k}}^N$, and hence the boundary between the weak- and strong-scattering regimes remains unchanged in the presence of the supercurrent. Moreover, with P_e around 1/2, the angular average of the momentum scattering time can be estimated by $\langle \tau_{\mathbf{k}}' \rangle = P_e (\tau_{\mathbf{k}}^N / P_e) + (1 - P_e) \tau_{\mathbf{k}}^N / (1 - P_e) = 2\tau_{\mathbf{k}}^N$. Then when $v_s \gtrsim 0.1k_F/m^*$, the SRT in the weak-scattering regime is enhanced to be two times of the one with $v_s = 0$, which agrees with the numerical calculation in Figs. 8(a) and 8(c) fairly well. It is emphasized that these estimations are based on the Fermi arcs, which are only established when $v_s \gtrsim 0.1k_F/m^*$.

Facilitated with these understandings, we then analyze the superconducting velocity dependencies of the SRT, explicitly shown in Fig. 8(c). When the superconducting velocity is small ($v_s \lesssim 0.1k_F/m^*$), there still exists considerable quasiparticle population in the region with $k_x > 0$. In this situation, the momentum scattering time increases from $\tau_{\mathbf{k}}^N$ to $2\tau_{\mathbf{k}}^N$ with the increase of the superconducting velocity. Hence, in the weak-(strong) scattering regime, the SRT increases (decreases) with the increase of the superconducting velocity. Whereas when $v_s \gtrsim 0.1k_F/m^*$, the physics can be simply understood based on the Fermi arc as addressed. Accordingly, in the weak-scattering regime, the SRT becomes two times of the one with $v_s = 0$, and remains unchanged with the increase of the superconducting velocity. However, in the strong-scattering regime, with the increase of the superconducting velocity, $\langle \Omega_{\mathbf{k}} \rangle_a$ decreases, and the module-dependent inhomogeneous broadening is suppressed. Hence, with the momentum scattering time relatively unchanged, the SRT in the strong-scattering regime increases with the increase of the superconducting velocity.

b. Branch-mixing-induced spin relaxation channel. We then focus on the quasiparticle spin relaxation with finite order parameter ($|\Delta| \gtrsim 0.1$ meV). We first explain the shift of the boundary between the weak- and strong scattering regimes due to the superconducting velocity when $|\Delta| = 0.5$ meV [Fig. 8(b)]. It is noticed that when $|\Delta| = 0.5$ meV with $v_s = 0$, from Eq. (37), one finds that the SOC around the Fermi momentum is markedly suppressed for the quasiparticles. Due to the supercurrent, before the blocking region appears ($v_s \lesssim 0.14k_F/m^*$), the quasiparticle populations are shifted away from the Fermi momentum. This enhances not only the inhomogeneous broadening but also the momentum scattering time due to the suppression of the phase space available for the quasiparticle scattering. Thus, when $v_s = 0.1k_F/m^*$, these two responses to the supercurrent jointly lead to the shift of the boundary between the weak- and strong-scattering regimes to a larger impurity density. Nevertheless, once the

blocking region forms (e.g., $v_s = 0.5k_F/m^*$), the influence of the superconducting velocity on the boundary between the weak- and strong-scattering regime is similar to the case with extremely small order parameter addressed above. Thus, when $v_s = 0.5k_F/m^*$ in Fig. 8(b), the boundary between the weak- and strong-scattering regimes remains unchanged.

We then analyze the superconducting velocity dependencies of the SRTs, shown in Fig. 8(d). Unlike the situation with an extremely small order parameter, the branch-mixing scattering can be efficiently triggered in the presence of the blocking region. Here, the role of the branch-mixing scattering on the quasiparticle spin relaxation is revealed by comparing the SRTs with and without the branch-mixing scattering. In Fig. 8(d), with the branch-mixing scattering switched off, in the strong- (weak) scattering regime, it is shown by the yellow (cyan) dashed curve with circles (crosses) that the SRTs are much larger than (comparable to) the ones with the branch-mixing scattering when $v_s \gtrsim 0.14k_F/m^*$. Hence the branch-mixing scattering plays dominant (marginal) role on the quasiparticle spin relaxation in the strong- (weak) scattering regime in the presence of the blocking region. It is noted that the spin relaxation channel due to the branch-mixing scattering resembles the one due to the intervalley scattering shown in our previous studies on the electron spin relaxations in monolayer rippled [105] and bilayer [106] graphene or monolayer MoS₂ [107].

Finally, we address a new feature in the weak-scattering regime when $|\Delta| = 0.5$ meV compared to the case with extremely small order parameter $|\Delta| = 0.01$ meV. In Fig. 8(d), one notices that when $|\Delta| = 0.5$ meV with $n_i/n_e = 0.005$, with the increase of the superconducting velocity in the region $0.1k_F/m^* \lesssim v_s \lesssim 0.3k_F/m^*$, the SRT is suppressed. This suppression of the SRT comes from the quasiparticle density dependencies on the superconducting velocity (refer to Fig. 5). When $0.1k_F/m^* \lesssim v_s \lesssim 0.3k_F/m^*$, the system lies in the crossover between the nondegenerate and degenerate limits. As predicted in the Brooks-Herring formula [108], in the nondegenerate regime, the momentum scattering due to impurities is enhanced with the increase of the quasiparticle density, owing to the increase of the phase space available for the quasiparticle scattering; whereas in the degenerate regime, the quasiparticle-impurity scattering becomes insensitive to the quasiparticle density [6,9]. Hence, when $v_s \gtrsim 0.1k_F/m^*$, the SRT first decreases and then becomes unchanged with the increase of the superconducting velocity.

V. CONCLUSION AND DISCUSSION

In conclusion, we have investigated the DP spin relaxation for the quasiparticle with a novel superconducting-velocity-tunable state in GaAs (100) QWs in proximity to an *s*-wave superconductor, by the KSBs derived in the quasiparticle approximation. In the superconducting QW, the superconducting velocity induced from the superconducting phase is shown to cause the tilt of the quasiparticle energy spectrum. It is found that when the quasiparticle energy spectrum is tilted to be smaller than the chemical potential, a blocking region corresponding to the negative excitation energy appears, which is in the crescent shape. The existence of the blocking region

can significantly influence the Cooper pairings, quasiparticle density and momentum current in QWs.

Specifically, the center-of-mass momentum \mathbf{q} is carried by the Cooper pairs, with the anomalous correlations only existing between the states with momentum $\mathbf{k} + \mathbf{q}/2$ and $-\mathbf{k} + \mathbf{q}/2$. Moreover, the Cooper pairings around the electron Fermi surface are efficiently suppressed. Furthermore, the quasiparticle density increases with the increase of the superconducting velocity. Particularly, the degenerate regime can be realized and the Fermi surface around the blocking region for the quasiparticles appears. The quasiparticle Fermi surface is constituted by the electron- and holelike Fermi arcs. Finally, it is revealed that when the blocking region appears, the momentum current contributed by the quasiparticles flows in the opposite direction to the one carried by the Cooper pairs. Thus, in the superconducting velocity dependence of the momentum current, a peak arises due to the competition of the Cooper pairs and quasiparticles in the blocking region, whose appearance corresponds to the emergence of the blocking region.

We then study the DP spin relaxation for the quasiparticles in the superconducting QWs by the KSBs. The KSBs for the quasiparticle is set up based on the quasiparticle approximation, in which the SOC and quasiparticle-impurity scattering are explicitly considered. By using the KSBs, the SRTs without and with the supercurrent are calculated. Rich physics is revealed. Without the supercurrent, we address that the branch-mixing scattering [36,37] due to the impurity is forbidden, indicating that the electron- and holelike branches are independent and hence only the intrabranched spin relaxation channel exists. In this situation, when $|\Delta|$ tends to zero, the SRT recovers to the normal one. Whereas with finite order parameter, we find that compared to the normal state, both the SOC and quasiparticle-impurity scattering are efficiently suppressed due to the *same* coherence factor $|\epsilon_{\mathbf{k}}|/\mathcal{E}_{\mathbf{k}}$. This leads to the enhancement of the SRT in both weak- and strong-scattering regimes with the boundary between the weak- and strong-scattering regimes unchanged.

When the supercurrent is turned on, the Fermi arc has intriguing effect on the DP spin relaxation, which exhibits very different physics depending on the magnitude of the order parameter. Specifically, when the order parameter is extremely small (e.g., $|\Delta| = 0.01$ meV), the branch-mixing scattering is still forbidden because the coherence factor ($\approx \epsilon_{\mathbf{k}}/|\epsilon_{\mathbf{k}}| + \epsilon_{\mathbf{k}'}/|\epsilon_{\mathbf{k}'}|$) tends to be zero in the quasiparticle-impurity scattering, indicating that the electron- and holelike Fermi arcs are independent. Anomalous features are revealed for the quasiparticle spin relaxation at the Fermi arc in the *strong* scattering regime. Specifically, on one hand, the spin oscillations can be induced by the superconducting velocity; on the other hand, the SRT becomes insensitive to the momentum scattering. The latter feature is in contrast to the motional narrowing feature in the conventional DP relaxation [40] in which the spin relaxation is suppressed by the momentum scattering.

With the *finite* order parameter ($|\Delta| \gtrsim 0.1$ meV), the situation becomes different. It is revealed that the tilt of the energy spectrum can trigger the branch-mixing scattering. In this situation, there exist not only the intrabranched spin relaxation channel, but also the interbranch one. Furthermore,

we reveal the role of the intra- and interbranch spin relaxation channels on the spin relaxation in both the weak- and strong scattering regimes. Specifically, in the weak-scattering regime, the intrabranch spin relaxation channel is dominant; whereas in the strong-scattering regime, the interbranch channel becomes dominant when the blocking region appears. Moreover, it is found that in contrast to the situation with an extremely small order parameter, in the strong-scattering regime, no spin oscillation occurs and the spin relaxation is suppressed by the momentum scattering.

Up till now, the predicted Fermi arc induced by the supercurrent has not yet been experimentally reported and we expect that our work will bring experimental attention. Nevertheless, it is noted that the experimental observation of the Doppler shift was realized in the Andreev reflection in the InAs QWs contacted by Nb electrodes [43]. Accordingly, one expects that for the superconducting-velocity-tunable quasiparticle state in the QWs, the suppressed Cooper pairings, large quasiparticle density, and nonmonotonically tunable momentum current can be directly measured, which reflects the information of the tilted quasiparticle energy spectrum and the emergence of the blocking region. For the quasiparticle spin relaxation, when the order parameter is extremely small as reported in Ref. [46] ($|\Delta| = 46 \mu\text{eV}$), in the presence of the supercurrent, the spin oscillations and the insensitiveness of the SRT on the impurity density can provide the evidence for the existence of the Fermi arcs; when the order parameter is finite, in the strong-scattering regime, the absence of the spin oscillations and the suppression of the SRT by the relatively large superconducting velocity (larger than the critical velocity) show the effect of the branch-mixing scattering on the quasiparticle spin relaxation.

Finally, we point out that the existence of the Fermi arcs can be markedly influenced by the dynamics of the quasiparticle condensation. It is important that the condensation rate is slower than the spin relaxation one. However, up till now, the details of the condensation process are not clear in superconductors [84–86], not to mention in the system proximity to a superconductor. Therefore the study on the spin dynamics and the existence of the Fermi arc can even shed light on the condensation process.

ACKNOWLEDGMENTS

This work was supported by the National Natural Science Foundation of China under Grant No. 11334014 and 61411136001, the National Basic Research Program of China under Grant No. 2012CB922002 and the Strategic Priority Research Program of the Chinese Academy of Sciences under Grant No. XDB01000000.

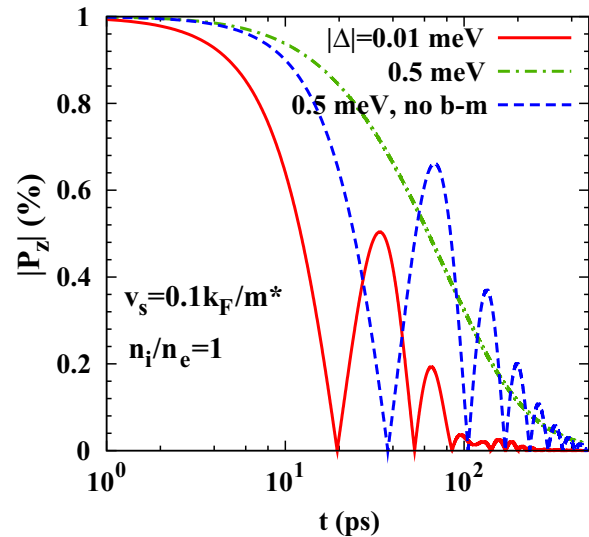


FIG. 9. Temporal evolution of the spin polarization in the strong scattering regime with extremely small order parameter $|\Delta| = 0.01 \text{ meV}$ (the red solid curve) and finite order parameter $|\Delta| = 0.5 \text{ meV}$ (the green chain curve). $v_s = 0.1 k_F / m^*$. The impurity density is $n_i / n_e = 1$, indicating that the system lies in the strong-scattering regime. The blue dashed curve represents the situation by switching off the branch-mixing scattering.

APPENDIX: SPIN OSCILLATIONS INDUCED BY SUPERCONDUCTING VELOCITY

In this appendix, we show the spin oscillations induced by the superconducting velocity in the strong-scattering regime with extremely small order parameter. It has been addressed in Sec. IV B 2 that the angular average of the effective magnetic field in one Fermi arc is not zero, which acts as an effective Zeeman field. Accordingly, even in the strong-scattering regime, this effective Zeeman field can lead to spin oscillations.

In Fig. 9, it is shown by the red solid curve that when the order parameter is extremely small ($|\Delta| = 0.01 \text{ meV}$), in the strong-scattering regime ($n_i / n_e = 1$) with the supercurrent ($v_s = 0.1 k_F / m^*$), the spin polarization oscillates in the temporal evolution. Whereas with a finite order parameter $|\Delta| = 0.5 \text{ meV}$, it is shown by the green chain curve that the oscillations vanish. This is because in the strong-scattering regime here, the triggered branch-mixing scattering becomes important. Thus the quasielectron can feel the SOC around the Fermi surface, whose angular average is exactly zero. By arbitrarily switching off the branch-mixing scattering, the spin oscillations of the spin polarization occur, shown by the blue dashed curve.

-
- [1] M. Eschrig, *Phys. Today* **64**, 43 (2011).
 - [2] J. Linder and J. W. A. Robinson, *Nat. Phys.* **11**, 307 (2015).
 - [3] M. Eschrig, *Rep. Prog. Phys.* **78**, 104501 (2015).
 - [4] *Optical Orientation*, edited by F. Meier and B. P. Zakharchenya (North-Holland, Amsterdam, 1984).
 - [5] *Semiconductor Spintronics and Quantum Computation*, edited by D. D. Awschalom, D. Loss, and N. Samarth (Springer, Berlin, 2002).
 - [6] I. Žutić, J. Fabian, and S. D. Sarma, *Rev. Mod. Phys.* **76**, 323 (2004).
 - [7] J. Fabian, A. M. Abiague, C. Ertler, P. Stano, and I. Žutić, *Acta Phys. Slov.* **57**, 565 (2007).
 - [8] *Spin Physics in Semiconductors*, edited by M. I. D'yakonov (Springer, Berlin, 2008).
 - [9] M. W. Wu, J. H. Jiang, and M. Q. Weng, *Phys. Rep.* **493**, 61 (2010).

- [10] T. Korn, *Phys. Rep.* **494**, 415 (2010).
- [11] *Handbook of Spin Transport and Magnetism*, edited by E. Y. Tsymbal and I. Žutić (CRC, Boca Raton, FL, 2011).
- [12] L. P. Gor'kov and E. I. Rashba, *Phys. Rev. Lett.* **87**, 037004 (2001).
- [13] F. S. Bergeret, A. F. Volkov, and K. B. Efetov, *Rev. Mod. Phys.* **77**, 1321 (2005).
- [14] A. I. Buzdin, *Rev. Mod. Phys.* **77**, 935 (2005).
- [15] F. S. Bergeret and I. V. Tokatly, *Phys. Rev. Lett.* **110**, 117003 (2013); *Phys. Rev. B* **89**, 134517 (2014).
- [16] T. Yu and M. W. Wu, *Phys. Rev. B* **93**, 195308 (2016).
- [17] C. Triola, D. M. Badiane, A. V. Balatsky, and E. Rossi, *Phys. Rev. Lett.* **116**, 257001 (2016).
- [18] H. L. Zhao and S. Hershfield, *Phys. Rev. B* **52**, 3632 (1995).
- [19] S. Takahashi, H. Imamura, and S. Maekawa, *Phys. Rev. Lett.* **82**, 3911 (1999).
- [20] S. Takahashi and S. Maekawa, *Phys. Rev. Lett.* **88**, 116601 (2002).
- [21] T. Yamashita, S. Takahashi, H. Imamura, and S. Maekawa, *Phys. Rev. B* **65**, 172509 (2002).
- [22] J. P. Morten, A. Brataas, and W. Belzig, *Phys. Rev. B* **72**, 014510 (2005).
- [23] N. Poli, J. P. Morten, M. Urech, A. Brataas, D. B. Haviland, and V. Korenivski, *Phys. Rev. Lett.* **100**, 136601 (2008).
- [24] S. Takahashi and S. Maekawa, *J. Phys. Soc. Jpn.* **77**, 031009 (2008).
- [25] H. Kontani, J. Goryo, and D. S. Hirashima, *Phys. Rev. Lett.* **102**, 086602 (2009).
- [26] H. Yang, S. H. Yang, S. Takahashi, S. Maekawa, and S. S. P. Parkin, *Nat. Mater.* **9**, 586 (2010).
- [27] F. Hübner, M. J. Wolf, D. Beckmann, and H. v. Löhneysen, *Phys. Rev. Lett.* **109**, 207001 (2012).
- [28] S. Takahashi and S. Maekawa, *Jpn. J. Appl. Phys.* **51**, 010110 (2012).
- [29] C. H. L. Quay, D. Chevallier, C. Bena, and M. Aprili, *Nat. Phys.* **9**, 84 (2013).
- [30] K. Ohnishi, Y. Ono, T. Nomura, and T. Kimura, *Sci. Rep.* **4**, 6260 (2014).
- [31] T. Wakamura, N. Hasegawa, K. Ohnishi, Y. Niimi, and Y. C. Otani, *Phys. Rev. Lett.* **112**, 036602 (2014).
- [32] T. Wakamura, H. Akaike, Y. Omori, Y. Niimi, S. Takahashi, A. Fujimaki, S. Maekawa, and Y. Otani, *Nat. Mater.* **14**, 675 (2015).
- [33] J. Linder and T. Yokoyama, *Phys. Rev. B* **83**, 012501 (2011).
- [34] I. Kulagina and J. Linder, *Phys. Rev. B* **90**, 054504 (2014).
- [35] S. A. Kivelson and D. S. Rokhsar, *Phys. Rev. B* **41**, 11693(R) (1990).
- [36] M. Tinkham and J. Clarke, *Phys. Rev. Lett.* **28**, 1366 (1972).
- [37] M. Tinkham, *Phys. Rev. B* **6**, 1747 (1972).
- [38] Y. Yafet, *Phys. Rev.* **85**, 478 (1952).
- [39] R. J. Elliott, *Phys. Rev.* **96**, 266 (1954).
- [40] M. I. D'yačkanov and V. I. Perel', *Zh. Eksp. Teor. Fiz.* **60**, 1954 (1971) [*Sov. Phys. JETP* **33**, 1053 (1971)].
- [41] H. Takayanagi and T. Kawakami, *Phys. Rev. Lett.* **54**, 2449 (1985).
- [42] T. Akazaki, H. Takayanagi, J. Nitta, and T. Enoki, *Appl. Phys. Lett.* **68**, 418 (1996).
- [43] F. Rohlfing, G. Tkachov, F. Otto, K. Richter, D. Weiss, G. Borghs, and C. Strunk, *Phys. Rev. B* **80**, 220507(R) (2009).
- [44] K. M. H. Lenssen, M. Matters, and C. J. P. M. Harmans, *Appl. Phys. Lett.* **63**, 2079 (1993).
- [45] T. D. Moore and D. A. Williams, *Phys. Rev. B* **59**, 7308 (1999).
- [46] Z. Wan, A. Kazakov, M. J. Manfra, L. N. Pfeiffer, K. W. West, and L. P. Rokhinson, *Nat. Commun.* **6**, 7426 (2015).
- [47] P. G. de Gennes and M. Tinkham, *Physics* **1**, 107 (1964).
- [48] G. Eilenberger, *Z. Phys.* **214**, 195 (1968).
- [49] A. I. Larkin and Y. N. Ovchinnikov, *Zh. Eksp. Teor. Fiz.* **55**, 2262 (1968) [*Sov. Phys. JETP* **28**, 1200 (1969)]; [*Zh. Eksp. Teor. Fiz.* **68**, 1915 (1975)] [*Sov. Phys. JETP* **41**, 960 (1975)] [*Zh. Eksp. Teor. Fiz.* **73**, 299 (1977)] [*Sov. Phys. JETP* **46**, 155 (1977)].
- [50] K. D. Usadel, *Phys. Rev. Lett.* **25**, 507 (1970).
- [51] G. M. Eliashberg, *Zh. Eksp. Teor. Fiz.* **61**, 1254 (1971) [*Sov. Phys. JETP* **34**, 668 (1972)].
- [52] A. Schmid and G. Schön, *J. Low Temp. Phys.* **20**, 207 (1975).
- [53] A. L. Shelankov, *Zh. Eksp. Teor. Fiz.* **78**, 2359 (1980) [*Sov. Phys. JETP* **51**, 1186 (1980)]; *J. Low Temp. Phys.* **60**, 29 (1985).
- [54] U. Eckern, *J. Low Temp. Phys.* **50**, 489 (1983).
- [55] J. Rammer and H. Smith, *Rev. Mod. Phys.* **58**, 323 (1986).
- [56] M. Y. Kuprianov and V. F. Lukichev, *Zh. Eksp. Teor. Fiz.* **94**, 139 (1988) [*Sov. Phys. JETP* **67**, 1163 (1988)].
- [57] N. Kopnin, *Theory of Nonequilibrium Superconductivity* (Oxford University Press, New York, 2001).
- [58] V. Chandrasekhar, in *The Physics of Superconductors*, edited by K. H. Bennemann and J. B. Ketterson (Springer-Verlag, Berlin, 2004), Vol. II.
- [59] Y. Takane, *J. Phys. Soc. Jpn.* **75**, 074711 (2006).
- [60] *Non-centrosymmetric Superconductors: Introduction and Overview*, edited by E. Bauer and M. Sigrist (Springer, Berlin, 2012).
- [61] F. Konschelle, *Eur. Phys. J. B* **87**, 119 (2014).
- [62] C. Espedal, P. Lange, S. Sadjina, A. G. Mal'shukov, and A. Brataas, [arXiv:1605.06611](https://arxiv.org/abs/1605.06611).
- [63] M. J. Stephen, *Phys. Rev.* **139**, A197 (1965).
- [64] P. Wölfle, *J. Low Temp. Phys.* **22**, 157 (1976).
- [65] D. Einzel and P. Wölfle, *J. Low Temp. Phys.* **32**, 19 (1978).
- [66] P. Wölfle and D. Einzel, *J. Low Temp. Phys.* **32**, 39 (1978).
- [67] A. G. Aronov, Yu. M. Gal'perin, V. L. Gurevich, and V. I. Kozub, *Adv. Phys.* **30**, 539 (1981).
- [68] R. Combescot, *Phys. Rev. A* **10**, 1700 (1974); *Phys. Rev. B* **13**, 126 (1976).
- [69] J. Hara and K. Nagai, *J. Low Temp. Phys.* **34**, 351 (1979).
- [70] S. Li, A. V. Andreev, and B. Z. Spivak, *Phys. Rev. B* **92**, 100506(R) (2015).
- [71] D. Einzel and L. Klam, *J. Low Temp. Phys.* **150**, 57 (2008).
- [72] L. Klam, D. Manske, and D. Einzel, in *Non-Centrosymmetric Superconductors*, edited by E. Bauer and M. Sigrist (Springer, Berlin, 2012).
- [73] J. D. Sau, R. M. Lutchyn, S. Tewari, and S. Das Sarma, *Phys. Rev. Lett.* **104**, 040502 (2010).
- [74] T. D. Stanescu, R. M. Lutchyn, and S. Das Sarma, *Phys. Rev. B* **84**, 144522 (2011).
- [75] H. Y. Hui, P. M. R. Brydon, J. D. Sau, S. Tewari, and S. Das Sarma, *Sci. Rep.* **5**, 8880 (2015).
- [76] J. Danon and K. Flensberg, *Phys. Rev. B* **91**, 165425 (2015).
- [77] H. Y. Kee, Y. B. Kim, and K. Maki, *Phys. Rev. B* **70**, 052505 (2004).

[78] I. Khavkine, H. Y. Kee, and K. Maki, *Phys. Rev. B* **70**, 184521 (2004).
 [79] G. Tkachov and V. I. Fal'ko, *Phys. Rev. B* **69**, 092503 (2004).
 [80] G. Tkachov, *Physica C* **417**, 127 (2005).
 [81] P. Fulde and R. A. Ferrell, *Phys. Rev.* **135**, A550 (1964).
 [82] A. I. Larkin and Yu. N. Ovchinnikov, *Zh. Eksp. Teor. Fiz.* **47**, 1136 (1964) [*Sov. Phys. JETP* **20**, 762 (1965)].
 [83] S. Takada and T. Izuyama, *Prog. Theor. Phys.* **41**, 635 (1969).
 [84] J. Bardeen, *Phys. Rev. Lett.* **9**, 147 (1962).
 [85] B. D. Josephson, *Phys. Lett.* **1**, 251 (1962).
 [86] M. Tinkham, *Introduction to Superconductivity* (McGraw-Hill, New York, 1975).
 [87] M. W. Wu and C. Z. Ning, *Eur. Phys. J. B* **18**, 373 (2000); M. W. Wu, *J. Phys. Soc. Jpn.* **70**, 2195 (2001).
 [88] G. Dresselhaus, *Phys. Rev.* **100**, 580 (1955).
 [89] A. L. Fetter and J. D. Walecka, *Quantum Theory of Many Particle Systems* (McGraw-Hill, New York, 1971).
 [90] G. D. Mahan, *Many Particle Physics* (Plenum, New York, 1990).
 [91] A. A. Abrikosov, L. P. Gorkov, and I. E. Dzyaloshinski, *Methods of Quantum Field Theory in Statistical Physics* (Prentice Hall, Englewood Cliffs, NJ, 1963).
 [92] *Semiconductors*, Landolt-Brnstein, New Series Vol. 17a, edited by O. Madelung (Springer, Berlin, 1987).
 [93] J.-M. Jancu, R. Scholz, E. A. de Andrada e Silva, and G. C. La Rocca, *Phys. Rev. B* **72**, 193201 (2005).
 [94] A. F. Andreev, *Sov. Phys. JETP* **19**, 1228 (1964).
 [95] G. E. Blonder, M. Tinkham, and T. M. Klapwijk, *Phys. Rev. B* **25**, 4515 (1982).
 [96] B. Pannetier and H. Courtois, *J. Low Temp. Phys.* **118**, 599 (2000).
 [97] P. Fulde, *Phys. Rev.* **137**, A783 (1965).

[98] S. Takada, *Prog. Theor. Phys.* **43**, 27 (1970).
 [99] H. Haug and A. P. Jauho, *Quantum Kinetics in Transport and Optics of Semiconductors* (Springer, Berlin, 1996).
 [100] P. Lipavský, V. Špička, and B. Velický, *Phys. Rev. B* **34**, 6933 (1986).
 [101] P. Zhang and M. W. Wu, *Phys. Rev. B* **84**, 045304 (2011).
 [102] T. Yu and M. W. Wu, *Phys. Rev. B* **93**, 045414 (2016).
 [103] The scattering term due to the interaction between quasielectrons is derived to be

$$\begin{aligned} \partial_T \rho_{\mathbf{k}}^{\text{q-e}}|_{\text{ee}} = & -\pi \sum_{\mathbf{k}'\mathbf{k}''} |V_{\mathbf{k}'-\mathbf{k}''}|^2 |I_{\mathbf{k},\mathbf{k}-\mathbf{k}'+\mathbf{k}''}|^2 |I_{\mathbf{k}'',\mathbf{k}'}|^2 \\ & \times \delta(E_{\mathbf{k}-\mathbf{k}'+\mathbf{k}''}^+ - E_{\mathbf{k}}^+ + E_{\mathbf{k}'}^+ - E_{\mathbf{k}''}^+) \\ & \times \{ (1 - \rho_{\mathbf{k}-\mathbf{k}'+\mathbf{k}''}^{\text{q-e}}) \rho_{\mathbf{k}}^{\text{q-e}} \text{Tr}[(1 - \rho_{\mathbf{k}'}^{\text{q-e}}) \rho_{\mathbf{k}''}^{\text{q-e}}] \\ & - \rho_{\mathbf{k}-\mathbf{k}'+\mathbf{k}''}^{\text{q-e}} (1 - \rho_{\mathbf{k}}^{\text{q-e}}) \\ & \text{Tr}[\rho_{\mathbf{k}'}^{\text{q-e}} (1 - \rho_{\mathbf{k}''}^{\text{q-e}})] \} + \text{H.c.}, \end{aligned}$$

with $\rho_{\mathbf{k}}^{\text{q-e}} = \frac{1+\tau_3}{2} \rho_{\mathbf{k}}^h$ being the density matrix for the quasi-electron. Here, $I_{\mathbf{k},\mathbf{k}'} = u_{\mathbf{k}} u_{\mathbf{k}'} - v_{\mathbf{k}} v_{\mathbf{k}'}$ is the coherence factor. From the scattering term, one sees that at low temperature, the quasiparticle-quasiparticle scattering is efficiently suppressed due to the coherence factor, which is proportional to $(\zeta_{\mathbf{k}}/\mathcal{E}_{\mathbf{k}})^4$ approximately.

[104] T. Yu and M. W. Wu, *Phys. Rev. B* **89**, 045303 (2014).
 [105] P. Zhang, Y. Zhou, and M. W. Wu, *J. Appl. Phys.* **112**, 073709 (2012).
 [106] L. Wang and M. W. Wu, *Phys. Rev. B* **87**, 205416 (2013).
 [107] L. Wang and M. W. Wu, *Phys. Lett. A* **378**, 1336 (2014); *Phys. Rev. B* **89**, 115302 (2014).
 [108] D. Rode, in *Semiconductors and Semimetals*, edited by R. K. Willardson and A. C. Beer (Academic, New York, 1975), Vol. 10, p. 1.